JOURNAL OF GEOPHYSICAL RESEARCH, VOL. 108, NO. B2, 2125, doi:10.1029/2000JB000118, 2003

Partial melting experiments on a MORB-like pyroxenite between 2 and 3 GPa: Constraints on the presence of pyroxenite in basalt source regions from solidus location and melting rate

Maik Pertermann[1,2] and Marc M. Hirschmann[1]

Received 21 December 2000; revised 6 June 2002; accepted 12 November 2002; published 27 February 2003.

[1] We present partial melting experiments at 2–3 GPa on a basaltic pyroxenite (G2) similar in composition to typical oceanic crust. The 3.0 GPa solidus is located at 1310 ± 12°C and the liquidus is 1500–1525°C. Clinopyroxene, garnet, quartz, and rutile are subsolidus phases. Garnet, quartz, and rutile are absent above 1475°C, 1365°C, and 1335°C, respectively. At the solidus, the garnet mode is low (18 wt.%) because clinopyroxene is unusually aluminous (13.8–15.5 wt.% Al_2O_3). In adiabatically upwelling mantle near 2–3 GPa, G2-like pyroxenite begins melting 35–50 km deeper than peridotite. The calculated near-solidus adiabatic productivity for G2 is ~13%/GPa and averages ~59%/GPa through the melting interval, suggesting substantial partial melting deep in basalt source regions: G2 is ~60% molten at the 3 GPa peridotite solidus. Small percentages of pyroxenite in the source significantly affect oceanic crust production and composition, as the proportion of pyroxenite-derived melt contributed to oceanic crust formation is 5 to >10 times the pyroxenite proportion in the source. Given the overall depleted isotopic character of mid-ocean ridge basalt (MORB), oversampling of fertile G2-like pyroxenite limits the abundance of such lithologies to ~<2% of the MORB source. Owing to high extents of partial melting, the effect of modest amounts of pyroxenite on Sm/Yb ratios of aggregated basalts is limited and depends largely on the average bulk composition of the pyroxenite source. Low near-solidus adiabatic productivities could allow small (~1–2%) proportions of basaltic pyroxenite to enhance (^{230}Th)/(^{238}U) in oceanic basalts without requiring marked shifts in other indicators of heterogeneity, such as Sr or Pb isotopes. *INDEX TERMS:* 3035 Marine Geology and Geophysics: Midocean ridge processes; 3630 Mineralogy and Petrology: Experimental mineralogy and petrology; 3640 Mineralogy and Petrology: Igneous petrology; *KEYWORDS:* pyroxenite melting, eclogite melting, MORB petrogenesis

Citation: Pertermann, M., and M. M. Hirschmann, Partial melting experiments on a MORB-like pyroxenite between 2 and 3 GPa: Constraints on the presence of pyroxenite in basalt source regions from solidus location and melting rate, *J. Geophys. Res.*, *108*(B2), 2125, doi:10.1029/2000JB000118, 2003.

1. Introduction

[2] Many have suggested that geochemical variations in basalts from oceanic islands [*Hofmann and White*, 1982; *Zindler et al.*, 1984; *Weaver*, 1991; *Hauri*, 1996], oceanic ridges [*Allègre and Turcotte*, 1986; *Lundstrom et al.*, 1995, 1999, 2000; *Hirschmann and Stolper*, 1996; *Niu and Batiza*, 1997; *Eiler et al.*, 2000], island arcs [*Feigenson and Carr*, 1993; *Schiano et al.*, 2000] and continental flood basalts [*Cordery et al.*, 1997; *Takahashi et al.*, 1998; *Yasuda and Fujii*, 1998] are in part a consequence of variable contributions of partial melts from olivine-poor heterogeneities such as pyroxenite, garnet pyroxenite, or eclogite. Some of these interpretations rely in part on correlations between major element and isotopic trends believed to be consistent with "pyroxenite" sources [*Hauri*, 1996; *Schiano et al.*, 2000] or on assumed partitioning of trace elements during partial melting of such sources [*Lundstrom et al.*, 1995; *Hirschmann and Stolper*, 1996; *Eiler et al.*, 2000; *Schiano et al.*, 2000]. However, the role of such lithologic heterogeneities in basalt petrogenesis remains controversial [e.g., *Bourdon et al.*, 1996a; *Stracke et al.*, 1999; *Kamber and Collerson*, 2000], in part because pyroxenite melting behavior is incompletely understood. Much of what is known about partial melting of eclogite and pyroxenite under nominally volatile-free (H_2O and CO_2 absent) conditions comes from some reconnaissance studies in the 1960s and 1970s (see review by *Hirschmann and Stolper* [1996]), and the recent work of *Yasuda et al.* [1994], *Hirschmann et al.* [1995], *Takahashi et al.* [1998], and *Yaxley and Green* [1998]. These studies establish that pyroxenite begins to melt at lower temperature than typical mantle peridotite, that partial melts of bulk compositions similar to that of basalt produce

[1]Department of Geology and Geophysics, University of Minnesota, Minneapolis, Minnesota, USA.
[2]Now at Institut für Mineralogie und Petrographie, Eidgenössische Technische Hochschule, Zürich, Switzerland.

0148-0227/03/2000JB000118$09.00

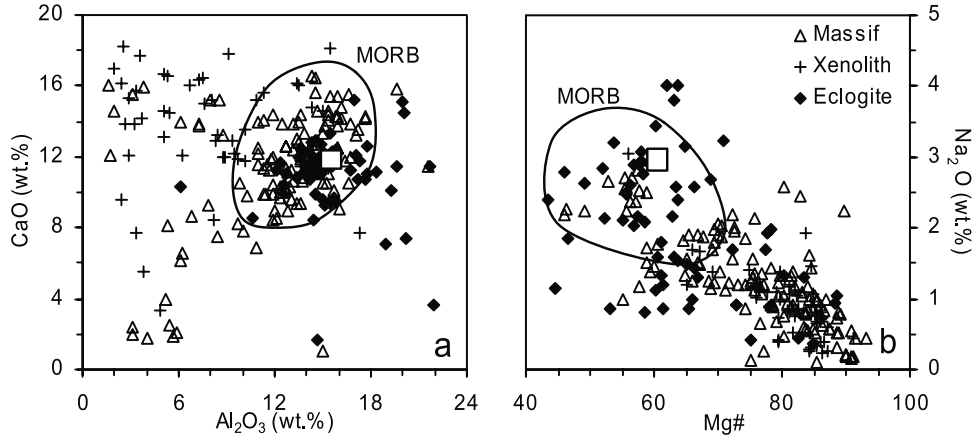

Figure 1. Comparison of the G2 bulk composition (open square) used in experiments with composition of MORB and of pyroxenites from peridotite massifs, xenoliths, and eclogites from the compilation of *Hirschmann and Stolper* [1996]. G2 pyroxenite is near the average of eclogite, having high total alkalis and low Mg# as well as average CaO and elevated Al_2O_3. It represents a relatively fertile bulk composition compared to pyroxenites from xenoliths and from orogenic massifs, which have lower alkalis and higher Mg#'s and are thus expected to be more refractory.

silicic partial melts, and that garnet is present along the pyroxenite solidus to pressures near 2 GPa. However, there are as yet no detailed partial melting studies of nominally dry pyroxenites, and much remains to be determined regarding pyroxenite in its melting interval. This includes the extent of melting, the composition of liquid, and the proportions of minerals in the residue. Each of these parameters may depend on pyroxenite composition, but at this time very little is known about this compositional dependence.

[3] Prior to investigation of the melting relations of possible lithologic heterogeneities in the shallow mantle, it is helpful to consider their likely compositions and hence their origins. The most commonly considered source for such heterogeneities are remnants of recycled oceanic crust [e.g., *Allègre and Turcotte*, 1986], though other origins are possible as well [*Hirschmann and Stolper*, 1996]. Major and trace element compositions of heterogeneities that do represent ancient oceanic crust could be fairly restricted and similar in many respects to modern oceanic crust, although oceanic gabbros span a wide range in major element compositions compared to mid-ocean ridge basalt (MORB) [e.g., *Dick et al.*, 1991; *Gillis et al.*, 1993; *Hekinian et al.*, 1993]. MORB-like compositions also represent a compositional extreme among plausible pyroxene-rich nominally volatile-free mantle lithologies, being high in Al_2O_3 and alkalis and low in MgO and Mg# (=molar Mg/(Mg + Fe) * 100) (Figure 1).

[4] In order to address the dearth of detailed experimental data on pyroxene-rich lithologies, we have performed high-pressure partial melting experiments at 2–3 GPa, conditions relevant to basalt petrogenesis beneath oceanic ridges and islands, on a composition similar to average modern oceanic crust. In this paper, we focus on the melting relations and the residual mineralogy of pyroxenite. We use these data to examine likely contributions of such lithologies to formation of basalt in the shallow mantle and to the possible influence on trace element and isotopic signatures of basalts. The new data provide constraints on the initial depth of pyroxenite melting in heterogeneous basalt source regions. A follow-up paper on the compositions of partial melts and residual minerals and their relationship to major element compositions of basalts is in preparation. In this paper "pyroxenite" is used for all pyroxene-rich, olivine-poor mantle heterogeneities and so, unless where otherwise specified, "pyroxenite" includes compositions otherwise considered to be eclogite or garnet-pyroxenite.

2. Experiments

2.1. Starting Material

[5] The starting mineral mixture (G2) was prepared from natural garnet and cpx that were separated from MORB-like eclogite W6.8 from the Münchberg Massif in Bavaria, Germany [*Stosch and Lugmair*, 1990] (sample courtesy of H.-G. Stosch). The separates were cleaned, ground, and then mixed with natural kyanite, quartz, and synthetic TiO_2 in proportions necessary to achieve the desired bulk composition. This was followed by firing at 1000°C in a CO/CO_2 gas mix at log $fO_2 \leq$ QFM to completely dehydrate the starting material. Finally, the G2 starting mix was ground again and passed through a 15 μm nylon screen. This assured uniformly small grain size and allowed sufficient intergrain and intragrain equilibration over a time interval practicable for piston cylinder experiments. Approximately 5 mg of the starting mix was fused to a glass in a graphite-lined Pt-capsule for 15 min in a piston cylinder run at 1.0 GPa and 1400°C. The starting mix composition was determined by analysis of this glass by electron microprobe (Table 1).

[6] The G2 composition is a reasonable approximation of subducted oceanic crust. We obtained the latter by assuming an average crustal thickness of 7 km, comprised of 0.5 km extrusives, 1.5 km dikes and 5 km gabbro, ignoring any sediment contribution (Table 1). As shown in Table 1, G2 is also very similar to the average oceanic gabbro and to average fresh fractionation-corrected basalt (H. Staudigel, personal communication, 2000). Table 1 also compares G2

Table 1. Composition of Starting Material[a]

	G2	Simpl. Crust	Gabbro	$MORB_8$	NAM-7	GA1
SiO_2	50.05	50.64	50.88	50.25	49.71	50.35
TiO_2	1.97	1.11	1.16	1.43	1.71	1.49
Al_2O_3	15.76	15.50	15.52	15.43	15.68	16.53
FeO	9.35	10.29	9.91	10.34	9.57	9.83
MnO	0.17	0.16	0.15	0.16	0.18	0.17
MgO	7.90	8.24	8.45	8.08	8.43	7.94
CaO	11.74	11.17	10.88	11.58	11.73	9.60
Na_2O	3.04	2.77	2.95	2.62	2.76	3.49
K_2O	0.03	0.12	0.10	0.10	0.23	0.44
Sum[b]	100.00	100.00	100.00	100.00	100.00	100.00
Mg#	60.1	58.8	60.3	58.2	61.1	59.0

[a]G2 is the starting material used in this study. Simpl. crust represents simplified oceanic crust and was obtained from preferred compositions of extrusives, dikes, and gabbros (H. Staudigel, personal communication, 2000) by assuming 0.5 km extrusives, 1.5 km dikes, and 5 km gabbro, weighted accordingly. Fresh, fractionation corrected $MORB_8$ and gabbro also shown for comparison (H. Staudigel, personal communication, 2000). NAM-7 and GA1 are starting materials of eclogite melting experiments by *Yasuda et al.* [1994] and *Yaxley and Green* [1998], respectively.

[b]GA1 sum includes 0.16 wt.% P_2O_5, all others normalized to 100 wt.%.

to bulk compositions from two previous studies on partial melting of anhydrous basaltic pyroxenite [*Yasuda et al.*, 1994; *Yaxley and Green*, 1998]. The composition used by *Yasuda et al.* [1994] is quite similar to G2, whereas the one used by *Yaxley and Green* [1998] is richer in total alkalis and much less calcic.

2.2. Piston Cylinder Experiments

[7] The phase equilibrium experiments were performed in an end-loaded piston cylinder apparatus at the Experimental Petrology Laboratory of the Department of Geology and Geophysics, University of Minnesota. The experimental assembly consisted of $BaCO_3$ sleeves, straight graphite heaters and internal spacers of crushable MgO. Temperatures were measured and controlled using W_3Re_{97}–$W_{75}Re_{25}$ thermocouples. All experiments were conducted using the hot piston-in technique with a pressure correction of −0.2 GPa, and pressure and temperature uncertainties are believed to be ±0.1 GPa and ±12°C, respectively [*Xirouchakis et al.*, 2001]. Graphite-lined Pt-capsules minimized Fe loss to the Pt container. Capsules filled with powdered rock were stored overnight at 300°C and welded shut immediately prior to the experiments. Additionally, the Pt-capsule was packed in a layer Fe_2O_3 powder as it was embedded in the MgO plug. The Fe_2O_3 acted as a getter to reduce the influx of hydrogen during experiments [*Robinson et al.*, 1998], thus further assuring near-anhydrous run conditions.

[8] At temperatures where melt fractions were expected to be small, vitreous carbon spheres of 80–147 μm diameter were included in the charge. The spheres form a melt segregation trap 3–4 layers high. This technique has been employed previously by *Robinson et al.* [1998] and *Pickering-Witter and Johnston* [2000] and is similar to the diamond aggregate technique [e.g., *Hirose and Kushiro*, 1993; *Baker and Stolper*, 1994], except that melt separation is driven by low surface tension between melt and spheres, rather than by a pressure gradient. The melt between the spheres equilibrates with the remainder of the charge by diffusion. The corresponding timescale for diffusive equilibration between the melt around the spheres and that in the residual silicate charge is on the order of 4–10 hours, assuming a diffusion coefficient of $\sim 10^{-8}$ cm/s^2. Runs employing vitreous carbon spheres were between 70 and 121 hours, except for run A195, at 3 GPa and 1400°C, which lasted 29 hours (Table 2).

[9] To determine the run times necessary to approach equilibrium, we conducted experiments at 3.0 GPa and 1335°C, ranging in duration from 6 to 121 hours. The melt composition in the vitreous carbon layer reached steady state in runs of ≥48 hours, but the mineral compositions remained heterogeneous and phase proportions calculated by mass balance calculations were variable. Backscatter electron images of longer runs show increased mineral homogeneity, although small relict cores (≤5 μm) remain in some cpx and garnet grains even after 121 hours (Figure 2). These cores have minor effect on phase equilibria and mass balance, as their relative mass is small. For example, unreacted 5 μm diameter cores in spherical grains of 10–15 μm in diameter represent only 12.5–3.7% of the crystal volume. Because such cores are not present in all grains, it appears that >90% of the mineral mass equilibrated with the matrix. Additionally, consistent calculated melt fractions (Table 2) suggest that equilibrium is approached at this temperature after about 70 hours. Shorter run times were employed at higher temperatures (≥1400°C), where the chief experimental problem encountered was minor Fe loss, equal to ~5% (relative) at 1400–1475°C and ~8% at 1500°C. Further evidence that the experiments approached equilibrium stems from the low sums of residual sums of squares in mass balance calculations (Table 2). The average from the 19 mass balanced experiments is 0.18, with a range of 0.007–0.59. This compares favorably to other experimental studies: e.g., *Falloon and Danyushevsky* [2000] reported an average of 0.2 (range 0.0009–0.7) for their 31 runs, and *Kinzler* [1997] reported a range from 0.01 to 1.2.

[10] Experiments were quenched by turning off the power to the heater while maintaining run pressure. After recovery of the assembly, the capsule position was determined to verify the correct position of the sample with respect to furnace hot spot and thermocouple. The capsules were then sectioned longitudinally and mounted in epoxy for polishing. Repeated vacuum impregnation with epoxy was necessary to counter plucking of vitreous carbon spheres and grains.

[11] Most experiments were conducted at 3.0 GPa, in the temperature range of 1300–1525°C, but some were done at 2.0 and 2.5 GPa and lower temperatures (Table 2). Modal proportions of the run products (Table 2 and Figure 3) were calculated by mass balance, using the methods of *Albarede and Provost* [1977].

3. Experimental Results

3.1. Phase Assemblages

[12] At 3.0 GPa, the subsolidus assemblage is cpx, garnet, quartz, and rutile. Glass was observed at 1315°C, but is not present in runs at 1300 or 1310°C. Below the solidus the minerals display few faceted grain boundaries and are significantly more heterogeneous compared to runs in which melt was present. Furthermore, rims of homogeneously quenched glass are absent around the vitreous carbon

Table 2. Summary of Experimental Conditions and Results[a]

Run No.	P (GPa)	T (°C)	t (hours)	Glass	Cpx	Garnet	Quartz	Rutile	Plag	res^2
A279[b]	2.0	1165	24		+	+	+	+	+	
A273[b]	2.0	1185	6	+	+	+	+	+	+	
A266[b]	2.0	1225	6	+	+	+		+	+	
A284[b]	2.0	1250	82	9.3 (2.7)	56.9 (1.3)	12.6 (1.1)		0 (0.2)	21.2 (1.2)	0.053
A184	2.0	1325	40	48.1 (1.1)	48.5 (1.4)	3.4 (1.1)				0.137
A252	2.0	1375	15	77.3 (1.2)	22.7 (1.1)					0.308
A202	2.5	1325	60.5	20.2 (1.3)	68.5 (1.9)	11.3 (1.1)				0.307
#166[b]	3.0	1300	92		78.2 (1.7)	17.8 (1.3)	3.7 (6)	0.3 (1)		0.135
A170[b]	3.0	1315	96	0 (3.2)[c]	79.1 (2.1)	17.4 (1.3)	3.2 (9)	0.3 (2)		0.212
A168[b]	3.0	1325	92	5.3 (1.3)	78.4 (1.7)	14.2 (1.0)	2.1 (5)			0.040
A177-6[b]	3.0	1335	6	+	+	+	+			
A177-12[b]	3.0	1335	12	+	+	+	+			
A177-24[b]	3.0	1335	24	+	+	+	+	trace		
A177-48[b]	3.0	1335	48	+	+	+	+			
A177-70[b]	3.0	1335	70	3.1 (1.3)	78.3 (1.7)	15.5 (1.1)	3.2 (5)			0.048
A177-82[b]	3.0	1335	82	7.4 (1.4)	76.3 (1.6)	14.5 (1.0)	1.6 (6)			0.075
A177-96[b]	3.0	1335	96	3.2 (1.3)	77.7 (1.7)	16.3 (1.1)	2.8 (5)			0.089
A177-121[b]	3.0	1335	121	2.0 (1.1)	78.7 (1.6)	16.1 (1.0)	3.3 (5)	trace		0.048
A171[b]	3.0	1350	77	7.9 (1.2)	76.5 (1.6)	14.0 (1.0)	1.6 (5)			0.007
A175[b]	3.0	1365	70.5	8.9 (1.4)	76.6 (1.7)	13.3 (1.1)	1.2 (5)			0.146
#164[b]	3.0	1375	72.5	17.9 (1.2)	70.5 (1.7)	11.6 (1.0)				0.037
A195[b]	3.0	1400	29	23.8 (1.3)	65.3 (1.7)	10.9 (1.2)				0.112
A189	3.0	1425	24	36.4 (1.3)	53.7 (1.5)	9.9 (1.0)				0.250
A190	3.0	1450	19	50.7 (1.1)	41.6 (1.3)	7.7 (9)				0.419
A194	3.0	1475	12	59.8 (1.4)	35.6 (1.5)	4.5 (1.0)				0.592
A197	3.0	1500	2.5	86.8 (1.5)	13.2 (1.5)					0.360
A199	3.0	1525	1.0	100						–

[a]Modes calculated by multiple linear regression techniques based on the study of *Albarede and Provost* [1977], with all oxides except MnO and K_2O, using a program written by M. B. Baker. "res^2" is the sum of the residual squares calculated using the modes obtained from the mass balance program to illustrate close attainment of equilibrium and facilitate comparison to other studies.

[b]Indicates runs with vitreous carbon spheres.

[c]Calculated melt fraction is zero, but melt observed in the vitreous carbon sphere layer. Note the large error compared to other low melt fraction runs. Mass balance by nonweighted least squares fit yields a melt fraction of 0.5%.

spheres at subsolidus conditions, and the spheres tended to pluck more easily. Cpx and an unidentified K-bearing aluminosilicate (possibly alkali feldspar) are in contact with the spheres at subsolidus conditions, and we believe that these are crystallized remnants of early disequilibrium partial melts.

[13] Cpx is present over the entire melting interval, whereas garnet is present up to 1475°C and quartz disappears above 1365°C. Rutile is observed above the solidus at 1315°C, and in two of the time series experiments at 1335°C (24 and 121 hours), but not in any of the other 1335°C runs or at 1325°C. We infer that rutile is stable from the solidus to at least 1335°C, as minerals with small (<1%) modes may elude detection in some cases. However, the presence of trace amounts of rutile has negligible effect on the mass balance, as is emphasized by the low sums of residual squares for these experiments (Table 2). The liquidus is

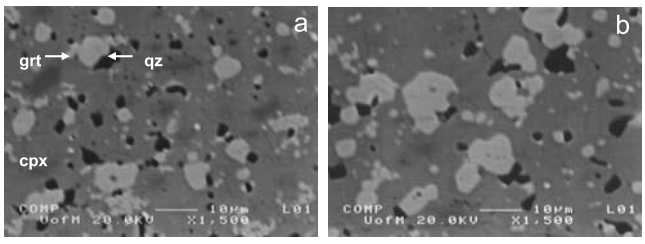

Figure 2. Backscatter electron images of time series experiments. (a) A177-24 (24 hours) and (b) A177-121 (121 hours). Note the easily visible zoning (dark patches) in the cpx in the shorter run. Considerably less zoning is visible in the experiment of longer duration. Also, note the increased overall grain size and the pronounced crystal faces of garnet in (b) compared to the shorter duration run (a).

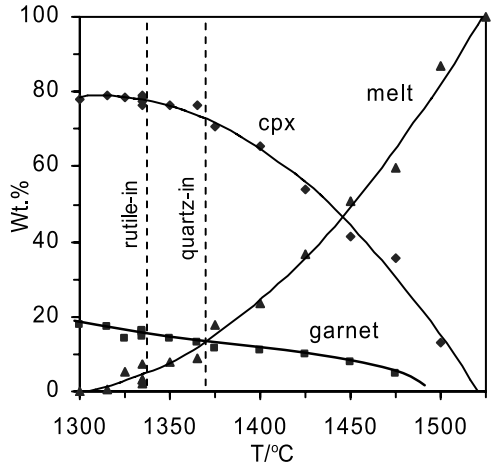

Figure 3. Modes of cpx, garnet, and melt calculated from mass balance of G2 partial melting experiments at 3 GPa. The solidus is at 1310 ± 12°C and the liquidus between 1500°C and 1525°C. Rutile is present to at least 1335°C, quartz is present to 1365°C, and garnet to 1475°C. Note the shallower slope of the melt fraction curve near the solidus and the overall low garnet mode, which reaches a maximum of 18% at the solidus. The melting interval of this fertile MORB-like pyroxenite composition is close to 200°C.

Table 3. Mineral Compositions From Experiments and the Literature[a]

	This Study							
	Garnet			Cpx			PH 2002 Cpx	HD 1993 Cpx
Run	A184	A168	A194	A184	A168	A194	A333	(low-Ti)
P (GPa)	2.0	3.0	3.0	2.0	3.0	3.0	3.0	3.0
T(°C)	1325	1325	1475	1325	1325	1475	1365	1380
n[b]	13	13	12	16	13	18	(19)	(10)
SiO_2[c]	39.89 (21)	39.07 (22)	40.21 (20)	48.59 (35)	50.02 (35)	50.31 (14)	50.11 (34)	49.17
TiO_2	0.80 (12)	1.01 (15)	0.72 (9)	1.23 (9)	1.87 (8)	0.71 (5)	2.64 (13)	0.98
Al_2O_3	23.20 (25)	22.41 (17)	23.06 (17)	14.10 (29)	15.09 (20)	14.64 (23)	16.68 (58)	14.14
FeO*	16.51 (60)	19.18 (22)	13.91 (35)	7.76 (16)	7.79 (12)	6.24 (13)	7.62 (17)	6.61
MnO	0.43 (6)	0.41 (3)	0.38 (3)	0.17 (3)	0.12 (3)	0.14 (3)	0.10 (3)	0.08
MgO	12.49 (60)	10.04 (11)	13.50 (39)	11.51 (17)	8.12 (12)	11.12 (23)	6.51 (24)	10.50
CaO	7.62 (27)	7.89 (27)	7.76 (20)	15.57 (13)	12.81 (19)	14.88 (18)	12.77 (77)	15.24
Na_2O	0.07 (4)	0.13 (3)	0.07 (2)	2.02 (8)	3.62 (7)	2.67 (11)	4.05 (11)	2.94
Sum	101.03 (33)	100.13 (36)	99.61 (28)	100.95 (32)	99.44 (36)	100.71 (27)	100.48 (60)	99.66
Mg#[d]	57.4	48.3	63.4	72.6	65.0	76.1	60.3	73.9
Jd[e]				0.14	0.25	0.18	0.28	0.21
CaTs[f]				0.18	0.08	0.16	0.06	0.16
CaEs[g]				0.03	0.12	0.06	0.16	0.02

[a]Mineral data from selected experiments and trace element partitioning studies. Mineral analyses from our experiments with electron microprobe at 15 kV, 7.5 nA, 30 s counting time on peaks, 15 s on each background, natural cpx, garnet, and hornblende as standards, ZAF correction.
[b]Number of analyses for each phase.
[c]Wt.% oxides, values in brackets are one standard deviation in terms of least units cited. Thus, 39.89 (21) should be read as 39.89 ± 0.21.
[d]Molar Mg/(Mg + Fe) * 100, all Fe assumed to be Fe^{2+}.
[e]Jadeite ($NaAlSi_2O_6$).
[f]CaTs ($CaAl_2SiO_6$).
[g]CaEs, Ca-Eskola ($Ca_{0.5}[\ ]_{0.5}AlSi_2O_6$). PH 2002: *Pertermann and Hirschmann* [2002]. HD 1993: *Hart and Dunn* [1993].

between 1500°C and 1525°C, as no crystals were observed at 1525°C. The partial melts are quartz and hypersthene normative and range in composition from basaltic at high melt fractions to andesitic near the solidus, where the SiO_2 concentration reaches 57.4 wt.%.

[14] Experimental charges at 2 GPa and 1325 and 1375°C consist of glass and cpx, with a small amount of garnet present in the 1325°C run. Mass balance yields a high proportion of glass in both runs and suggests that garnet is present until approximately 50% melting, compared to 60% at 3 GPa. The persistence of garnet to such a high melt fraction at 2 GPa contrasts with the absence of garnet in peridotite near its solidus below ~2.8 GPa [e.g., *Robinson and Wood*, 1999] and strongly reaffirms the enhanced stability of garnet in pyroxenitic lithologies. At 2 GPa and 1250°C plagioclase (An_{37}) is present in addition to cpx, garnet, and rutile. Both garnet and plagioclase were identified in 2 GPa experiments that bracketed the solidus (1165–1225°C), but quartz was seen only at 1185°C and below.

3.2. Phase Compositions

[15] Electron microprobe analyses of cpx and garnet from selected experiments are given in Table 3. The garnets have nearly constant CaO concentrations, deviating little from 8 wt.%, regardless of temperature or pressure, but become less magnesian with increasing pressure. Clinopyroxenes from the 3.0 GPa experiments are Na, Al, and Ti rich and show systematic compositional shifts with temperature and pressure: with increasing temperature, CaO increases and Al_2O_3, TiO_2, and Na_2O decrease. The Mg# ranges from 65 up to 79. With increasing pressure, the principal shift is an increase in Na_2O.

[16] The most notable compositional feature of the pyroxenes is the high Al_2O_3 content, which ranges from 13.8 to 15.5 wt.%. The high aluminum content is a consequence of multiple aluminous components, including Jd ($NaAlSi_2O_6$), CaTs ($CaAl_2SiO_6$), $Ca(Mg_{0.5},Ti_{0.5})AlSiO_6$ (alumino-buffonite) [*Sack and Ghiorso*, 1994] and, $Ca_{0.5}[\ ]_{0.5}AlSi_2O_6$ (Ca-Eskola component, CaEs) [*Smyth*, 1980; *McCormick*, 1986]. At 3 GPa, the range of component concentrations are (mol. fraction, with increasing *T*): Jd 0.15–0.27, CaTs 0.18–0.08, Al-buffonite 0.10–0.04, and CaEs 0.13–0.04 (see caption of Table 3 for calculation of components), meaning there are up to 6% vacancies in the M2 site. A detailed description of the compositions and petrologic significance of these unusual vacancy-rich pyroxenes, together with explicit mineral and melt compositions as a function of temperature and pressure will be published in the forthcoming contribution.

3.3. Solidus Location and Temperature Versus Melt Fraction Behavior

[17] At 3 GPa, the solidus of the G2 pyroxenite is 1310 ± 12°C and the temperature interval between solidus and liquidus spans approximately 200°C. The melt fraction versus temperature trend is not linear (Figure 3), as the isobaric melt productivity, $(\partial F/\partial T)_P$, increases with rising temperature. At 2 GPa, the solidus is located at 1175 ± 12°C and extrapolation of our *T* versus *F* data suggests that the liquidus is near 1415 ± 15°C. Thus the melting interval at 2 GPa is larger than that at 3 GPa.

[18] *Yaxley and Green* [1998] found significant amounts of melt at 1250–1300°C and 3.5 GPa in their MORB pyroxenite partial melting experiments. Their solidus location is therefore well below that of G2 at 3 GPa, probably owing to high K_2O in their GA1 starting material (Table 1). At 3 GPa the solidus of NAM-7 (Table 1), a bulk composition quite similar to G2 [*Yasuda et al.*, 1994], is between 1250 and 1300°C and the liquidus is between 1400 and 1450°C, in general agreement with *Yaxley and Green*'s

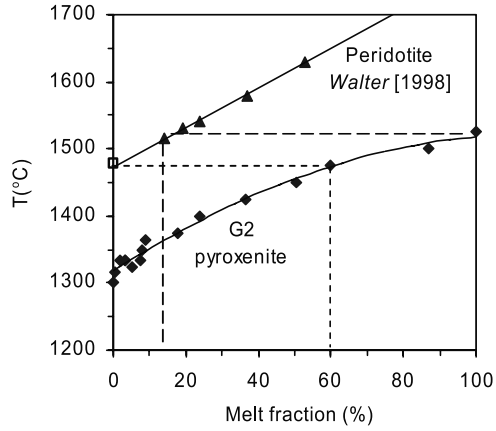

Figure 4. Comparison of pyroxenite and peridotite melting at 3.0 GPa. The trend of melt fraction versus temperature for the peridotite partial melting data of *Walter* [1998] intersects the solidus at 1480 ± 20°C, in agreement with the solidus parameterization of *Hirschmann* [2000], which is marked with an open square. The solidus of G2 pyroxenite, 1310 ± 12°C, is therefore 170 ± 25°C cooler than the peridotite solidus at this pressure. Note that the pyroxenite is almost 60% melted at the temperature of the peridotite solidus and completely melted when the peridotite is >20% molten.

[1998] and our experiments, given pressure and temperature uncertainties of multianvil devices.

[19] The solidus of G2 pyroxenite at 2 and 3 GPa is respectively 190 ± 25°C and 170 ± 25°C cooler than that of peridotite (1360 ± 20°C and 1480 ± 20°C) [*Walter*, 1998; *Hirschmann*, 2000; *Herzberg et al.*, 2000]. In Figure 4, we compare the melt fraction versus temperature trend of our pyroxenite with similar data for peridotite from the study of *Walter* [1998]. At the temperature of the peridotite solidus, the G2 pyroxenite has a melt fraction of almost 60% and garnet is no longer stable. Thus, basaltic pyroxenite, if present, will be largely melted before the peridotite solidus is reached. As discussed below, this will have considerable influence on the trace element signature derived from a pyroxenitic component in basalt source regions. Our results also validate models that assume that pyroxenitic bodies can undergo significant partial melting in environments such as extending continental lithosphere, where geotherms are elevated but not hot enough to produce partial melts of nominally anhydrous peridotite [e.g., *Leeman and Harry*, 1993; *Carlson and Nowell*, 2001].

[20] Our data allow estimation of the difference in onset of melting for upwelling of a mixed peridotite/pyroxenite mantle. Note that these estimates only apply to pyroxenite similar in major element composition to G2 pyroxenite; heterogeneities with different bulk compositions could have cooler or hotter solidus temperatures. For an adiabatic gradient of 10°C/GPa [e.g., *Ita and Stixrude*, 1992], the 3 GPa solidus of G2 corresponds to a potential temperature of 1280°C. Applying the peridotite solidus parameterization of *Hirschmann* [2000], peridotite partial melting begins at 1.4 GPa along this adiabat, which corresponds to a depth 50 km less than the G2 pyroxenite solidus. A similar offset applies to an adiabat passing through the 2 GPa pyroxenite solidus. The large offset between G2 pyroxenite and peridotite solidi indicates that partial melting of pyroxenites should begin in the vicinity of at least 100 km depth beneath ridges, which is similar to the likely depths of dehydrogenation melting discussed by *Hirth and Kohlstedt* [1996]. Thus, pyroxenites should be considered as a potential source of partial melts believed to be present in the deeper parts of MORB source regions on the basis of tomographic inversions from the MELT experiments [*Toomey et al.*, 1998].

3.4. Isobaric and Adiabatic Melt Productivity

[21] The low isobaric melt productivity indicated near the solidus at 3 GPa corresponds approximately to the melting interval in which quartz ± rutile are present in the residue (Figure 3 and Table 2). Based on thermodynamic calculations and analogies to simple systems, *Hirschmann et al.* [1999] predicted low isobaric melt productivity for near-solidus partial melting of peridotite. Though strong evidence for low $(\partial F/\partial T)_P$ has not been documented in near-solidus peridotite partial melting experiments, the low productivity observed here most likely stems from a similar mechanism to that hypothesized for peridotite. Both systems have assemblages with low thermodynamic variance in which the liquids are able to coexist with the residual minerals over a range of temperatures owing mainly to changes in liquid composition associated with near-solidus concentration of incompatible elements in the liquid (mainly K_2O in this case). Pyroxenites with assemblages of higher thermodynamic variance may therefore be expected to display higher $(\partial F/\partial T)_P$ near the solidus.

[22] The experimental melt fraction versus temperature trend (Table 2) can be fit to an empirical polynomial (Figure 5a)

$$F = 100\left(aT'^2 + bT'\right) \tag{1}$$

where F is in units of percent and T' is the normalized temperature,

$$T' = (T - T_{\text{solidus}})/\left(T_{\text{liquidus}} - T_{\text{solidus}}\right). \tag{2}$$

T_{liquidus} and T_{solidus} are assumed to be linear functions of pressure

$$T_{\text{liquidus}} = c + dP(\text{GPa}); \tag{3}$$

$$T_{\text{solidus}} = e + fP(\text{GPa}). \tag{4}$$

We optimized the parameters a through f via a least squares scheme, using the temperature and melt fraction data in Table 2 and the following constraints on the liquidus and solidus temperatures: At 3 GPa we assume that T_{solidus} equals 1310°C and that T_{liquidus} is in the interval between 1500 and 1525°C; at 2 GPa we assume that T_{solidus} is in the interval between 1165 and 1185°C and that T_{liquidus} is in the interval between 1400 and 1430°C. The resulting parameterization, shown in Figure 5a, with values of parameters given in the caption, reproduces all the melt fraction data within experimental uncertainty.

[23] Near the solidus of G2 pyroxenite, this parameterization of melt fraction yields an estimated isobaric productivity, $(\partial F/\partial T)_P$, of 0.12%/°C, which is higher than those

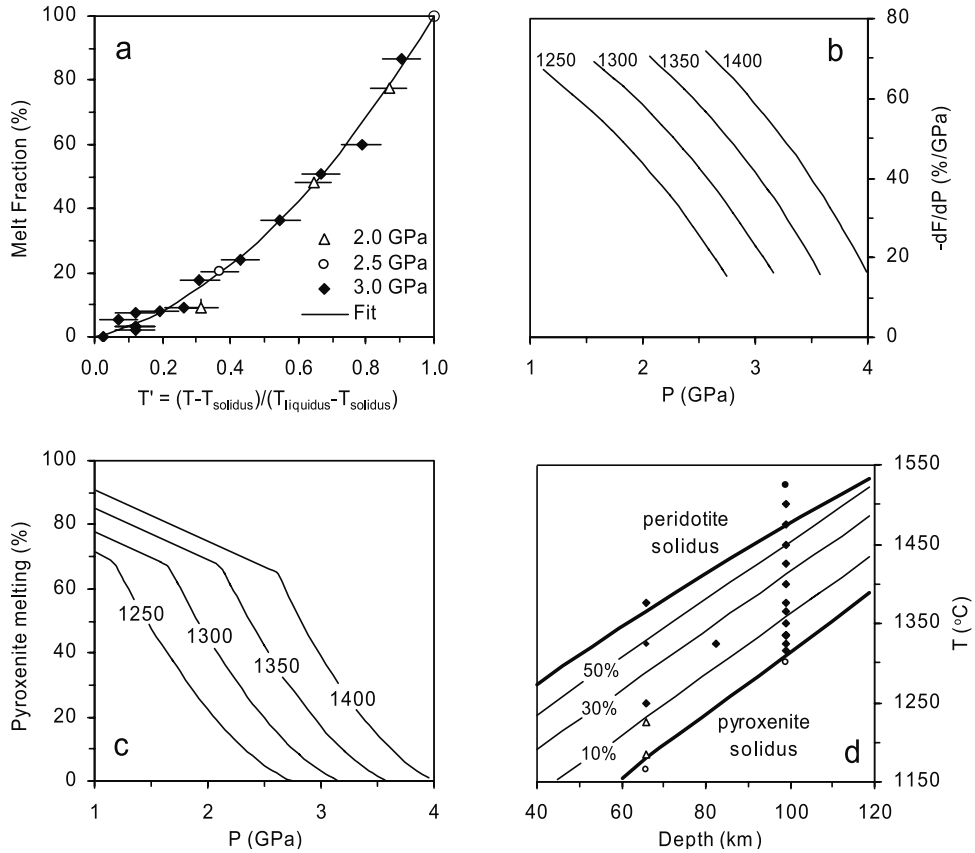

Figure 5. (a) Melt fraction (F) in percent from the G2 partial melting experiments plotted against scaled temperature T', defined as $T' = (T - T_{solidus})/(T_{liquidus} - T_{solidus})$ and compared to a fitted trend given by $F = 100(aT'^2 + bT')$, with the pyroxenite liquidus given by $T_{liquidus} = c + dP$ and solidus given by $T_{solidus} = e + fP$, where a = 73.68, b = 26.32, c = 1175°C, d = 114°/GPa, e = 920°C, and f = 130°/GPa. (b) G2 pyroxenite solidus and isopleths of pyroxenite melt fraction inferred from the parameterization defined in (a) in the region cooler than the peridotite solidus [*Hirschmann*, 2000]. (c) Calculated melt fraction for adiabats with a range of potential temperatures. Below the peridotite solidus, the adiabat is assumed to be 10°C/GPa and melt productivity is taken from parameterization described above; above the peridotite solidus, pyroxenite productivity is assumed to have a constant value of 16.5%/GPa. (d) Calculated adiabatic productivity, in %/GPa, for a range of potential temperatures in the region where only pyroxenite is above its solidus. Filled diamonds show experiments in which melt fraction has been determined (Table 2), filled circle shows supersolidus experiment, open triangles show melt-present experiments that lack quantitative melt fraction estimates, and open circles show subsolidus experiments.

calculated from thermodynamic models for peridotite near its solidus (<0.1) [*Hirschmann et al.*, 1999], but less than that applicable to peridotite over much of its melting interval (~0.2%/°C) [e.g., *Langmuir et al.*, 1992; *Kinzler and Grove*, 1992; *Baker and Stolper*, 1994]. With increasing melt fraction, the isobaric productivity of G2 pyroxenite grows progressively, reaching approximately 0.8%/°C as the liquidus is reached.

[24] The melt fraction parameterization also allows estimates of melt production for pyroxenite veins or blobs melting in the depth interval where surrounding peridotite remains below its solidus. For the case where the pyroxenite/peridotite ratio is small, the geothermal gradient is governed by the adiabat of upwelling peridotite, which is ~10°C/GPa [e.g., *Ita and Stixrude*, 1992], and the calculation represents a maximum, as increasing proportions of pyroxenite will cause progressive cooling and reduced melting per increment of upwelling [*Sleep*, 1984; *Hirschmann and Stolper*, 1996; *Phipps Morgan*, 2001]. As shown in Figure 5b, the average pyroxenite adiabatic productivity over this pressure interval increases from ~15%/GPa near the pyroxenite solidus to ~70%/GPa near the intersection of each adiabat with the peridotite solidus, with the latter calculated from the study of *Hirschmann* [2000]. These productivities are comparable to those modeled by *Hirschmann and Stolper* [1996] (50–66%/GPa) and are much greater than typical adiabatic productivity of peridotite, which may be quite variable, but is generally less than 16.5%/GPa [*Asimow et al.*, 2001].

[25] High productivities for pyroxenite are expected for regions deeper than the onset of significant peridotite partial melting. Because of the large difference between the peridotite solidus and that of G2 pyroxenite, large extents of pyroxenite partial melting (>60%) are expected as the

peridotite solidus is approached (Figures 5c and 5d). Once the peridotite begins to melt, the pyroxenite should have a reduced productivity [*Hirschmann and Stolper*, 1996; *Phipps Morgan*, 2001]. Assuming a productivity of 16.5%/GPa for pyroxenite partial melting in the region of peridotite partial fusion [*Hirschmann and Stolper*, 1996], G2 pyroxenite will undergo nearly complete fusion if it ascends to near-Moho depths (Figure 5c).

3.5. Small Garnet Mode and Cpx Compositions in Partially Molten Pyroxenite

[26] Two striking features of the partial melting relations of G2 pyroxenite are the relatively small mode of garnet ($\leq$18%) and the highly aluminous pyroxene compositions (up to 15.5 wt.%) (Table 3). As illustrated in Figure 6, these features are related to one another by a mass balance relationship. Near the solidus at 3 GPa the highly aluminous, subcalcic pyroxenes approach the bulk composition of the pyroxenite, so that lever rule considerations require only a small garnet mode. Although pyroxenes are less aluminous at higher temperatures, garnet melts preferentially relative to cpx, decreasing the garnet mode and increasing Al_2O_3 in partial melts.

[27] Comparison of our results to previous eclogite partial melting experiments suggests that the high Al_2O_3, and by inference, small garnet modes, are a general feature of nominally anhydrous eclogites over a wide range of pressures. For example, clinopyroxenes with 14.5–15 wt.% Al_2O_3 have been reported at 3.5 GPa by *Yaxley and Green* [1998] and at 5 and 7.5 GPa by *Yasuda et al.* [1994]. *Johnston* [1986] reported cpx with up to 17 wt.% from basalt crystallization experiments at 3 GPa. To our knowledge, all hyperaluminous clinopyroxenes from pyroxenite partial melting experiments have a significant CaEs component, which in turn requires high silica activity [*Wood and Henderson*, 1978]. Pyroxenites that partially melt to form liquids with low silica activities are thus not expected to have similarly aluminous residual pyroxenes and so could allow for larger garnet modes.

[28] The relatively low mode of garnet and the highly aluminous pyroxenes in G2 near the 3 GPa solidus contrast with the garnet modes typical of tectonically exposed eclogites. These commonly have garnet/cpx ratios close to unity and clinopyroxenes with Al_2O_3 usually not exceeding 10–12 wt.% (e.g., see the study of *Carswell* [1990] for a review of eclogite facies rocks). However, clinopyroxenes from some eclogitic xenoliths found in kimberlites have Al_2O_3 concentrations similar to or even greater than those documented here [*Smyth*, 1980; *McCormick*, 1986; *Snyder et al.*, 1997; *Harlow*, 1999], presumably reflecting a combination of equilibration at high temperatures and pressures, as well as aluminous bulk compositions.

[29] Trace element and isotopic models of partial melting of MORB or subducted oceanic crust at high pressure generally assume mineral modes with cpx/grt ratios of 50/50 to 70/30 [e.g., *Hirschmann and Stolper*, 1996; *Stracke et al.*, 1999; *Eiler et al.*, 2000]. Our results indicate that such large garnet modes are probably not attained by volatile-free partial melting of basaltic compositions, and that models incorporating such modes exaggerate the role of garnet in lithologies similar to MORB. Note, however, that large garnet modes are likely at lower temperatures and pressures, where coexisting clinopyroxenes are not as aluminous. Thus, we expect that dehydration melting of subducted oceanic crust (either in the Archean or for the presumed source of present-day adakites) yields less aluminous pyroxene compositions and consequently higher garnet modes. For example, *Rapp and Watson* [1995] observed up to ~40 wt.% garnet near the dehydration solidus of basaltic amphibolite at 2.7–3.2 GPa [see *Rapp and Watson*, 1995, Figure 3].

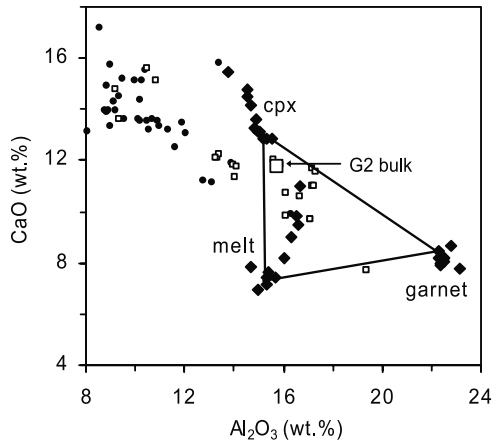

Figure 6. Compositions of cpx, garnet, and melt from partial melting experiments. This plot illustrates graphically the relationship between the bulk composition of G2 and the mineral compositions from the experiments. It shows that the G2 bulk composition is close to that of the very Al-rich, subcalcic cpx and relatively distant from garnet, which requires a low gt/cpx modal ratio. With increasing *T*, partial melts approach the bulk composition and garnet mode diminishes. The solid lines connect phases for a low-*T*, near-solidus assemblage, emphasizing the resulting low overall garnet mode. Cpx from natural eclogites (solid black circles, from tectonically exposed eclogites [*Clarke et al.*, 1997; *Sisson et al.*, 1997; *DiVincenzo et al.*, 1997]; open small squares from xenoliths in kimberlite [*Smyth*, 1980; *McCormick*, 1986; *Snyder et al.*, 1997; *Harlow*, 1999]) are generally less aluminous and more calcic, thereby resulting in the large characteristic garnet modes in natural eclogites of basaltic bulk composition.

4. Discussion

4.1. Reaction of Pyroxenite Partial Melts With Surrounding Peridotite

[30] Although it is established that pyroxenite heterogeneities present in upwelling mantle may begin partial melting at considerable depths, the fate of such melts and their consequences for the geochemistry of erupted basalts remain poorly constrained. Because partial melts of silica-saturated pyroxenite are not in equilibrium with olivine, *Yaxley and Green* [1998] and *Yaxley* [2000] concluded that such melts would crystallize when reacted with surrounding mantle, destroying the pyroxenite partial melt and increasing the opx mode and the trace element fertility of the surrounding peridotite. Such reactions may not be expected for silica-undersaturated partial melts of pyroxenite [*Hirsch-*

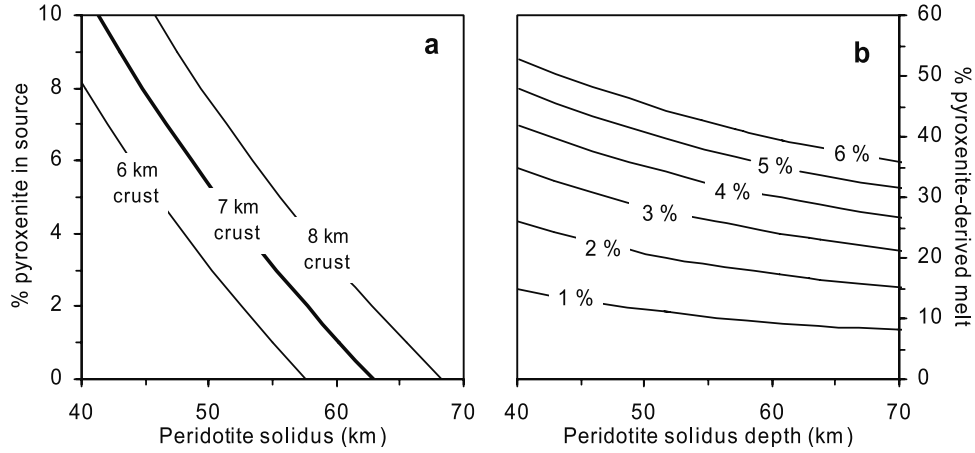

Figure 7. (a) Proportion of pyroxenite in the MORB source region that can be present without exceeding a given thickness (6 and 8 km) of crust formation at the ridge, calculated for 2-D integration of melts generated by passive upwelling beneath a ridge [after *Plank and Langmuir*, 1992]. Peridotite and pyroxenite solidi are calculated at variable mantle potential temperature according to the study of *Hirschmann* [2000] and to (4), respectively, and melting ends at a depth of 10 km. Pyroxenite partial melting is calculated according to (1)–(4) in the region deeper than the peridotite solidus and is assumed to be 16%/GPa at shallower depths. Peridotite melts at the rate of 13%/GPa to $F = 0.2$ and thereafter with a reduced melting rate of 5%/GPa. Note that only small proportions of pyroxenite can be accommodated unless the onset of peridotite melting is very shallow. (b) Proportion of oceanic crust derived from pyroxenite source as a function of peridotite solidus for varying pyroxenite volumes (1–6%) in the source region.

mann et al., 1995; *Lundstrom et al.*, 2000], but will certainly occur if high silica activity melts come into contact with olivine. However, we note that silica-saturated lithologies are themselves not in equilibrium with peridotite and we presume that opx-rich subsolidus reaction skarns (or a high pressure equivalent) will develop well before the initiation of partial melting [*Kogiso et al.*, 2000]. Such websteritic skarns will be thin, owing to the sluggishness of solid-state diffusion [*Hofmann and Hart*, 1978], but should insulate siliceous melts from reaction with olivine until the melts are segregated from their source. Segregation by reactive infiltration [*Kelemen et al.*, 1995; *Daines and Kohlstedt*, 1993; *Lundstrom et al.*, 2000] will be inhibited because percolating partial melts coming into contact with olivine are likely to crystallize, thereby inhibiting further percolation [*Chadam et al.*, 1976].

[31] The melt extraction mechanism for chemically isolated pyroxenite bodies is poorly understood, but a recent analysis by *Kogiso et al.* [2000] suggests that partial melts can escape their source without equilibration with surrounding peridotite, provided that the source is greater than 0.1–1 m wide. Once partial melts segregate from pyroxenite bodies, their fate depends on the mechanism of transport. Extensive interaction with overlying peridotite would lead to crystallization, as suggested by *Yaxley and Green* [1998]. Such freezing-in would have little effect on the incompatible trace element budgets of melts extracted from heterogeneous source regions because subsequent partial melting of peridotite will ultimately release them to the magmas extracted from the region. Major elements and compatible elements could be profoundly affected by such interactions. However, the occurrence in erupted oceanic basalts of radiogenic Os, which is strongly compatible and apparently derived from pyroxenite sources, suggests that such melts are in some instances extracted with only limited interaction with peridotite [*Hauri*, 1997; *Kogiso et al.*, 2000]. The mechanisms of such transport remain uncertain.

4.2. Melting and Crust Production at Oceanic Ridges

[32] Solidus locations and productivities estimated above allow us to appraise the relative contributions of pyroxenite and peridotite to crust production at mid-ocean ridges. We assume an adiabatic passive upwelling regime [*Plank and Langmuir*, 1992], with chemically independent but thermally equilibrated pyroxenite and peridotite sources. A preliminary evaluation of the permissible proportion of pyroxenite in the source regions of normal oceanic crust (6–8 km) [*White et al.*, 1992] can be made by allowing the peridotite solidus to vary and solving for the amount of pyroxenite permissible without exceeding crustal thickness observations.

[33] Figure 7a shows the relationship between peridotite solidus depth and G2 pyroxenite proportion that produces 6–8 km of crust, based on the parameterization of (1)–(4). With increasing depth of the peridotite solidus, the required volume of pyroxenite diminishes rapidly. If peridotite partial melting begins deeper than 70 km, no appreciable component similar to G2 pyroxenite can be present, but if peridotite partial melting begins at 40 km, more than 10% pyroxenite is permissible. If the spinel peridotite solidus is assumed to be 60 km, which corresponds to a mantle potential temperature of 1340°C [*Hirschmann*, 2000], 0.4–3.9% pyroxenite can be tolerated. As previously noted by *Hirschmann and Stolper* [1996], the volume of oceanic crust originating from pyroxenite greatly exceeds the volume of pyroxenite originally present in the source region. For deep peridotite solidi, this volume ratio is in the range of 4–6, but for cooler adiabats, it can be greater than 10

(Figure 7b). Thus, a few percent of pyroxenite in basalt source regions may result in significant enhancements in crustal production and produce a sizable fraction of melt in MORB.

[34] The actual amounts of pyroxenite in the source regions of MORB and most other common basalts must be reconciled with the geochemistry of the lavas. Geochemical constraints depend partly on the assumed trace element and isotopic budget of the pyroxenite. Given the predominance of the depleted isotopic component in MORB [*Zindler and Hart*, 1986], we think it unlikely that normal MORB derives from a source with more than 2–3% pyroxenite with phase relations similar to G2. For example, Sr and Pb concentrations in typical altered MORB are 110 and 0.3 ppm, respectively [*McCulloch and Gamble*, 1991], but about 40% and 85%, respectively, are likely removed by subduction processes [*Kogiso et al.*, 1997a], yielding a bulk composition with 66 ppm Sr and 0.045 ppm Pb. Alternatively, whole rock analyses of pyroxenite veins from alpine peridotite massifs give 43 ± 0.3 ppm Sr (n = 49) [*Bodinier et al.*, 1987; *Suen and Frey*, 1988; *Pearson et al.*, 1993] and 0.13 ± 0.08 ppm Pb (n = 16) [*Hamelin and Allègre*, 1988]. These values can be compared to 10 ppm Sr and 0.018 ppm Pb in the depleted mantle (DM) (S. Jacobsen, personal communication, 2000). Therefore, if a MORB source region consists of peridotite with DM concentrations of Sr and Pb, $^{87}Sr/^{86}Sr = 0.7022$, and $^{206}Pb/^{204}Pb = 17.6$, and pyroxenite with 66 ppm Sr, 0.13 ppm Pb, $^{87}Sr/^{86}Sr = 0.705$, and $^{206}Pb/^{204}Pb = 22$, one can calculate the compositions of the resulting aggregated basalts assuming that Sr and Pb are sufficiently incompatible to leave negligible concentrations in the melting residue. For 2% pyroxenite and 98% peridotite and 7 km of crust generation, the result is $^{87}Sr/^{86}Sr = 0.7027$ and $^{206}Pb/^{204}Pb = 18.45$, well within the domain of typical MORB, but 4% pyroxenite yields aggregated liquids more radiogenic than most MORB ($^{87}Sr/^{86}Sr = 0.7032$ and $^{206}Pb/^{204}Pb = 19.29$).

[35] We note that the calculations in Figure 5 and in the paragraph above are based on the experimentally determined solidus and productivity of G2 pyroxenite. Other pyroxenite compositions have solidi closer to that of peridotite [e.g., *Kogiso et al.*, 2001], and even G2 pyroxenite may produce less melt if melt is removed as upwelling proceeds [e.g., *Asimow et al.*, 1997]. If pyroxenites present in basalt source regions are more refractory than G2 or if they melt fractionally, their proportion present in basalt source regions could be greater than the 2–3% limit we estimate here.

4.3. Geochemistry of Basalts Derived From a Heterogeneous Mantle

[36] Near-total fusion of a pyroxenitic component has important consequences for apparent mixing relations in basalts derived from heterogeneous source regions. For example, if we consider a mantle source that has a given proportion of such highly fertile peridotite and that attains conditions appropriate for partial melting of volatile-poor peridotite, the *absolute* contribution from pyroxenite to the incompatible trace element and isotope budget of aggregated melts will be effectively constant, regardless of the degree of melting of the peridotite portion of the source. Thus, the *relative* contribution from pyroxenite will diminish with increasing extent of melting of the peridotite. This lends support to the hypothesis that a single mantle source can produce isotopically enriched melts when there is little or no peridotite fusion and isotopically depleted melts when there is extensive melting of peridotite [*Sleep*, 1984; *Phipps Morgan and Morgan*, 1999; *Phipps Morgan*, 1999, 2001].

[37] In detail, a heterogeneous mantle containing highly fusible bodies similar to G2 pyroxenite would behave quite differently from previous models of blended melts from such sources. Such models have assumed a more refractory pyroxenite behavior and therefore incorporate contributions from pyroxenite that are at most 3–4 times source abundance [*Hirschmann and Stolper*, 1996; *Stracke et al.*, 1999; *Phipps Morgan*, 2001], rather than the 5 to >10 estimated here for melting beneath ridges (Figure 7b). Also, because the enhancement ratio (the proportion of melt derived from pyroxenite divided by the proportion of pyroxenite in the source) is high owing to partial melting in the region deeper than the peridotite solidus (and not from high productivity in the region where peridotite is also partially melting), it must diminish as peridotite fusion progresses. For pyroxenite-like G2, models where the enhancement ratio is assumed to be constant [e.g., *Stracke et al.*, 1999] likely produce inaccurate estimates of the consequences of partially melting a mixed lithology mantle, as variations in in situ melt fractionation of the pyroxenite-derived melt are overestimated. We emphasize, however, that the range of plausible pyroxenite compositions, which may occur in the mantle, is considerable and that more refractory compositions would not melt so extensively as G2, although the enhancement ratio should still diminish with the extent of peridotite partial melting.

5. Trace Element and Isotope Signatures in MORB Derived From a Pyroxenite/Peridotite Source

5.1. Overview

[38] Because trace element and isotopic distinctions between ancient subducted crust and the depleted mantle are believed to be substantial [e.g., *Zindler et al.*, 1984; *Allègre and Turcotte*, 1986; *Hauri*, 1996; *Kogiso et al.*, 1997a, 1997b], the presence of recycled material in mantle source regions may have a significant effect on basalt geochemistry. Similar statements can be made for pyroxenite with different origins. In addition to the direct effects of source variations, trace element and isotopic variations in oceanic basalts may be influenced by differences in melting behavior between pyroxenites and peridotites. This provides one possible explanation for observed correlations between geochemical characteristics indicative of source composition and those that are controlled by fractionations occurring during partial melting [e.g., *Lundstrom et al.*, 2000]. *Hirschmann and Stolper* [1996] suggested that pyroxenites could be responsible for some of the trace element and isotope fractionations believed to be indicative of garnet in the source, including Hf-Nd isotope systematics [*Salters and Hart*, 1989], $(^{230}Th)/(^{238}U)$ disequilibria [*Beattie*, 1993], and REE element patterns, as expressed by Sm/Yb ratios [*Shen and Forsyth*, 1995; *Hirschmann and Stolper*, 1996]. Because their partial melting behavior has not been well established previously, pyroxenites' role in generating gar-

net signatures has remained unclear. For example, some have assumed that a garnet pyroxenite component enhances (^{230}Th)/(^{238}U) [*Lundstrom et al.*, 1995, 1999, 2000; *Bourdon et al.*, 1996a; *Hirschmann and Stolper*, 1996], but others regard pyroxenite as easily fusible and with limited selectivity between Th and U, leading to low (^{230}Th)/(^{238}U) [*Stracke et al.*, 1999].

[39] In this section, we apply our experimental results to consider the effect of pyroxenite similar to G2 on Sm/Yb ratios and (^{230}Th)/(^{238}U) of mantle-derived melts and we present model calculations to address the effect of a mixed peridotite/pyroxenite source on formation of typical oceanic crust. Important considerations include the mode of garnet in the residue, as discussed above, and the partitioning of relevant trace elements between clinopyroxene and liquid. It should be emphasized again that the calculations are directly applicable to pyroxenite similar to our G2 composition but that *other* pyroxenites could behave differently.

[40] To explore the Sm/Yb characteristics of oceanic crust generated from passive upwelling of a mixed pyroxenite/peridotite source, we calculate integrated melts in a manner similar to the study of *Hirschmann and Stolper* [1996]. We calculate liquid Sm and Yb concentrations by assuming integrated fractional melting. We recognize that this is not technically compatible with the melt productivity functions derived from our experiments (1)–(4) (Figure 5), which are strictly applicable to batch melting. Melt segregation is likely to diminish melt production, and so will produce more effective separation of Sm from Yb, meaning calculated Sm/Yb of pyroxenite-containing sources are minima. Similarly, calculated extents of melting, productivities, and crustal thicknesses are maxima.

5.2. Calculations and Parameter Considerations

[41] We have already discussed the relative extents of melting expected for decompression melting of coexisting peridotite and pyroxenite lithologies, and the expected low modal garnet in MORB-like pyroxenite, but several additional parameters must be constrained prior to evaluation of the potential role of garnet pyroxenite on the Sm/Yb and (^{230}Th)/(^{238}U) of average MORB. The bulk composition of the pyroxenite is critical for Sm/Yb calculations, but is less crucial for calculated (^{230}Th)/(^{238}U), for which efficiency of melt segregation and the rate of partial melting during upwelling, (dF/dP) are key. Selecting appropriate partition coefficients is important for both calculations.

[42] The trace element composition of pyroxenitic lithologies in the convecting mantle may be quite variable [*Hirschmann and Stolper*, 1996], so we consider four model bulk compositions: subducted oceanic crust (SOC) and average pyroxenite (AVG), both from the study of *Hirschmann and Stolper* [1996], average NMORB from the study of *McCulloch and Gamble* [1991], and the dehydrated subducted oceanic crust residue (DAK) from experiments of *Kogiso et al.* [1997a] (Table 4). For simplicity, we assume that all pyroxenites have the same mineral modes and melting behavior as G2. Of course, pyroxenites similar to alpine massifs and xenoliths (AVG pyroxenite) would be expected to be more refractory (Figure 1) and probably also have different mineral modes, but we use the AVG trace element concentrations to help illustrate the importance of pyroxenite source composition on the resulting basalt geochemistry.

Table 4. Model Compositions of Depleted Mantle and Pyroxenites[a]

	DM	SOC	AVG	NMORB	DAK
Sm (ppm)	0.317	2.321	1.42	3.752	4.72
Yb (ppm)	0.432	3.05	1.55	3.9	4.43
Sm/Yb	0.734	0.761	0.916	0.962	1.065
Sm/Yb$_{DM}$		1.037	1.248	1.311	1.452
U (ppm)	0.22	0.136			

[a]DM (depleted mantle), SOC (subducted oceanic crust), and AVG (average composition of pyroxenites from xenoliths and alpine peridotite massifs from the study of *Hirschmann and Stolper* [1996]. NMORB = altered NMORB from the study of *McCulloch and Gamble* [1991] and DAK = averaged dehydrated amphibolite residue from the study of *Kogiso et al.* [1997a].

[43] In calculations of U-series disequilibria, elevated (^{230}Th)/(^{238}U) in basalt requires separation of melt from the source at low porosities in the presence of a phase that preferentially retains U. Melt extraction from small pyroxenite heterogeneities may be different than from peridotite and could occur at relatively large porosities, thereby limiting elevation in (^{230}Th)/(^{238}U). However, this may depend on the dimensions of the body and on the mechanism of melt extraction, both of which are known poorly. Here we apply the dynamic model of *McKenzie* [1985] and *Williams and Gill* [1989] and assume that melt extraction can occur at low porosity (0.1%). If this assumption is incorrect, then the calculated (^{230}Th)/(^{238}U) are maxima. The magnitude of ^{230}Th excess in a dynamic model depends on the rate of melting dF/dP, which we take from the parameterization in Figure 5. Development of ^{230}Th excess from the model of *Spiegelman and Elliott* [1993] would also depend strongly on the initial productivity, though in a more complex fashion than a dynamic model. In the following calculations, the two types of models would give qualitatively similar results.

[44] Owing to the lack of cpx/melt partition data available for mineral compositions similar to those from the G2 experiments, we investigated trace element partitioning for appropriate vacancy-rich aluminous cpx in a related study [*Pertermann and Hirschmann*, 2002]. The resulting partition coefficients are distinct from those previously assumed to be applicable to partial melting of pyroxenite. For example, *Salters and Longhi* [1999] and *Stracke et al.* [1999] assumed that cpx/liquid partitioning of Th and U in pyroxenitic systems is best approximated by those for the aluminous cpx reported by *Hauri et al.* [1994], but these are an order of magnitude larger than those relevant to partial melting of pyroxenite with vacancy-rich cpx [*Pertermann and Hirschmann*, 2002]. Further details of the partition coefficients applied for Sm/Yb and (^{230}Th/^{238}U) calculations are given in the captions to Figures 8–10. Note that we ignore the effect of rutile on Th and U partitioning owing to a dearth of constraints and the low rutile mode (0.3%), although there is evidence suggesting that rutile strongly retains U [*Dardon et al.*, 2001], thus potentially enhancing U/Th fractionation from partial melting of G2-like pyroxenite.

5.3. Sm/Yb in MORB

[45] Sm/Yb in regionally averaged MORB, when normalized to the composition of the depleted mantle (Table 4), is typically 1.3–1.5 [*Hofmann*, 1988; *White et al.*, 1992;

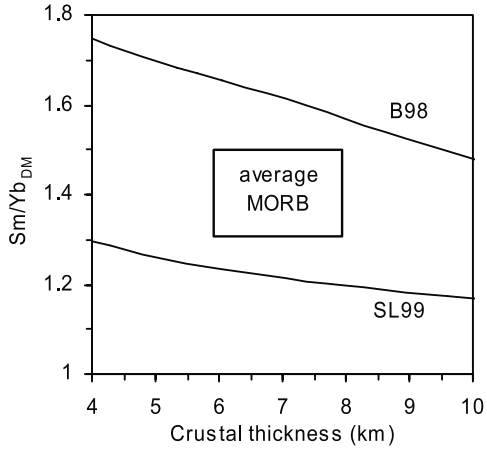

Figure 8. Calculated Sm/Yb (normalized to DM) (Table 4) as a function of crustal thickness for spinel peridotite melting using an integrated fractional melting model and the peridotite melting regime described in Figure 7. Mineral modes are ol 0.56, opx 0.30, and cpx 0.14, and we neglect the presence of spinel. Two sets of coefficients are used for cpx: *Blundy et al.* [1998] (D_{Sm} = 0.67, D_{Yb} = 1.43) and *Salters and Longhi* [1999] (averaged from all reported runs: D_{Sm} = 0.217, D_{Yb} = 0.331). According to *Blundy et al.* [1998], HREE are compatible in aluminous cpx, and this results in enhanced calculated Sm/Yb. Partition coefficients for ol and opx are from the studies of *Kennedy et al.* [1993] and *Salters and Longhi* [1999], respectively. Results are relatively insensitive to the peridotite mineral modes. Calculations with modes of ol 0.6, opx 0.25, and cpx 0.25 using the *Salters and Longhi* [1999] partitioning data for cpx and yielding 7 km of crust produce Sm/Yb$_{DM}$ of 1.25, just slightly higher than the value, 1.21, calculated with 14% cpx and still less than the range, 1.3–1.5, typical of MORB [*Hofmann*, 1988; *White et al.*, 1992; *Shen and Forsyth*, 1995].

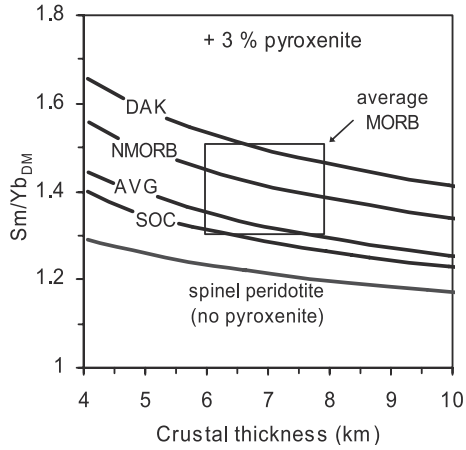

Figure 9. Calculated Sm/Yb ratios (normalized to DM) of integrated oceanic crust as a function of the peridotite solidus depth for a mixed peridotite/pyroxenite mantle with variable proportions of pyroxenite. The calculation is compared to Sm/Yb$_{DM}$ and typical thickness of oceanic crust and is similar to that in Figure 8, except that the mantle is considered to consist of spinel peridotite with a variable proportion of pyroxenite. Calculations with 3% pyroxenite are identical except that different initial trace element compositions are assumed (Table 4): SOC, subducted oceanic crust pyroxenite; AVG, average pyroxenite [both from *Hirschmann and Stolper*, 1996]; NMORB, average NMORB [*McCulloch and Gamble*, 1991]; DAK, dehydrated subducted oceanic crust residue [*Kogiso et al.*, 1997a]. These are compared to calculated melting of pure spinel peridotite, calculation as in Figure 8. Pyroxenite and peridotite melting are treated separately, and the resulting melts are assumed to mix before injection of the magma into the oceanic crust. We assume that garnet-out in pyroxenite coincides with the peridotite solidus, but more complicated models using the end-member assumptions of garnet-out in pyroxenite at 40 and 80% melting, independent of the peridotite solidus location, give essentially the same results. Sources for ranges of Sm/Yb$_{DM}$ and crustal thickness of typical oceanic crust are as in Figure 8. Owing to large extents of melting of fertile G2 pyroxenite, Sm/Yb fractionations are modest and the effect of variable pyroxenite proportion in the source is related principally to its assumed Sm/Yb ratio. Partition coefficients for peridotite are taken from the study of *Salters and Longhi* [1999] (see Figure 8), those for pyroxenite are as follows: garnet, D_{Sm} = 0.275, D_{Yb} = 3.6 [averaged from runs 8 and 11 of *Van Westrenen et al.*, 1999]; cpx, D_{Sm} = 0.198, D_{Yb} = 0.369 [*Pertermann and Hirschmann*, 2002]. We note that X_{Ca} of our garnets in the 3.0 GPa runs is 0.22 ± 0.01, which is above the critical value of X_{Ca} = 0.19 of *Van Westrenen et al.* [2001]. According to *Van Westrenen et al.* [2001], garnets with X_{Ca} > 0.19 should have compatible HFSE. However, Ti is relatively incompatible in our garnets (D_{Ti} = 0.18 ± 0.04), and therefore we believe that the low-Ca garnets of runs 8 and 11 (X_{Ca} = 0.18 and 0.16, respectively) of *Van Westrenen et al.* [1999] are representative of REE partitioning behavior of garnet in our study.

Shen and Forsyth, 1995]. These elevated ratios have been attributed to the presence of garnet during MORB petrogenesis [*Bender et al.*, 1984; *Frey et al.*, 1993; *Shen and Forsyth*, 1995]. If the mantle solidus is encountered at a depth sufficient to generate 7 km crust (~70 km) (Figure 7), peridotite is in the spinel facies [*Robinson and Wood*, 1999]. If the partition coefficients of *Salters and Longhi* [1999] are applied, integrated liquids from partial melting of spinel peridotite beginning at this depth have Sm/Yb$_{DM}$ of 1.35 (Figure 8), which is insufficient to account for the range of Sm/Yb$_{DM}$ observed in typical MORB. Alternatively, if the partition coefficients of *Blundy et al.* [1998] are used, integrated liquids have Sm/Yb$_{DM}$ of 1.62 (Figure 8), which illustrates *Blundy et al.*'s [1998] contention that REE patterns in MORB may not require garnet in the source. The difference in the two calculations highlights the challenge in constraining the possible effect of garnet pyroxenite on Sm/Yb (or equivalently, Lu/Hf) ratios, as the composition of melt extraction from a baseline pyroxenite-absent source is poorly constrained. If the partition coefficients of *Blundy et al.* [1998] are most appropriate, so-called garnet signatures may not be useful as indicators of the presence or absence of garnet pyroxenite, as has been previously suggested [e.g., *Hirschmann and Stolper*, 1996; *Bourdon et al.*,

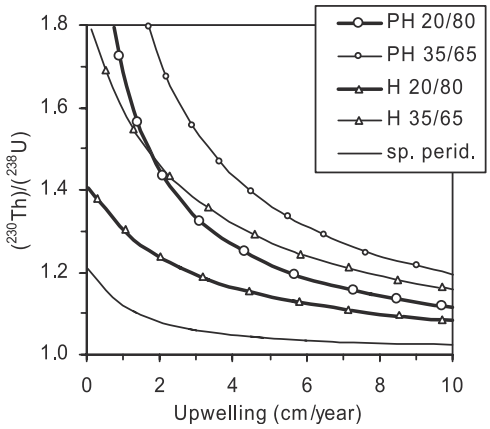

Figure 10. Calculated (^{230}Th)/(^{238}U) generated from partial melting of G2 pyroxenite domains upwelling in a mantle dominated by peridotite, following the models of *McKenzie* [1985] and *Williams and Gill* [1989]. In these models, only the melting rate at the onset of partial melting is relevant, and we assume a pyroxenite productivity (16.5%/GPa) appropriate for near-solidus melting of pyroxenite (Figure 5d). Also shown is (^{230}Th)/(^{238}U) from partial melting of spinel peridotite, calculated in the same fashion, but with productivity of 11%/km. Values of model parameters include porosity = 0.1%, pyroxenite density = 3550 kg/m^3, peridotite density = 3300 kg/m^3, and melt density = 2800 kg/m^3. For pyroxenite, two alternative sets of cpx/liquid partition coefficients are used: one set is averaged from the experiment of *Pertermann and Hirschmann* [2002] (D_U = 0.0029, D_{Th} = 0.0026) and the other is from the 2.5 GPa experiment of *Hauri et al.* [1994] (D_{Th} = 0.014, D_U = 0.0127. Garnet/liquid *D*s for pyroxenite are taken from run 11 of *Van Westrenen et al.* [1999] (D_U = 0.046, D_{Th} = 0.011). The spinel peridotite curve is calculated with 30% opx and 14% cpx and the averaged partition coefficients of *Wood et al.* [1999]. Garnet pyroxenite is assumed to have 20% grt and 80% cpx. Also shown are results for 35% grt and 65% cpx, which illustrates the effect of an elevated garnet mode. The calculations use the same garnet *D*s and either the cpx *D*s of *Pertermann and Hirschmann* [2002] (PH) or *Hauri et al.* [1994] (H). All calculated partial melts of garnet pyroxenite have greater (^{230}Th)/(^{238}U) than that from spinel peridotite at a given upwelling rate. Garnet pyroxenites with large garnet modes may not have vacancy-rich cpx, and so the aluminous cpx partition coefficients of *Hauri et al.* [1994] may be most appropriate. If this is the case, then the competing effects of changing mineral mode and changing partition coefficients may nearly cancel, yielding similar effects on (^{230}Th)/(^{238}U).

1996a; *Stracke et al.*, 1999]. If less extreme fractionations are realistic for spinel peridotite [e.g., *Gaetani and Watson*, 2000], garnet may be required. However, the relationship between pyroxenite abundance and Sm/Yb ratios may still be difficult to determine, as we will illustrate next.

[46] As shown in Figure 9, small fractions of pyroxenite in the source could elevate the calculated Sm/Yb$_{DM}$ of MORB for a given peridotite solidus depth, but the influence is relatively modest and depends on pyroxenite composition. Note that a highly fertile pyroxenite such as G2 undergoes large degrees of melting, which limits in situ Sm/Yb fractionation, and the pyroxenite bulk trace element content strongly affects the formation of a "garnet signature." The influence of highly fusible pyroxenite on the Sm/Yb or Lu/Hf ratios of basalt is therefore difficult to anticipate without prior knowledge of bulk trace element concentrations. Stronger fractionations may derive from a more refractory pyroxenite, which would begin melting closer to the peridotite solidus and therefore would not achieve such large total extents of melting.

5.4. (^{230}Th)/(^{238}U) in MORB

[47] At one time garnet was thought to be the only mineral in basalt source regions that could account for observed ^{230}Th excesses in MORB and OIB [*Beattie*, 1993], but *Wood et al.* [1999] argued that high-pressure aluminous pyroxene could also be responsible. *Chabaux and Allègre* [1994], *Lundstrom et al.* [1995, 1999, 2000], *Hirschmann and Stolper* [1996], and *Condomines and Sigmarsson* [2000] suggested that garnet pyroxenites may account for observed elevated (^{230}Th)/(^{238}U) > 1 in MORB. Though garnet pyroxenite may not be required if *Wood et al.* [1999] are correct, an important unresolved question is the relationship, if any, between mantle heterogeneity and melting processes that are reflected by (^{230}Th)/(^{238}U).

[48] Data from MORB give apparently conflicting evidence on the relationship between mantle heterogeneity and melting processes. On a global and local scale, (^{230}Th)/(^{238}U) in MORB are positively correlated with trace element indicators of source heterogeneity such as Th/U and K/Ti [*Bourdon et al.*, 1996a; *Lundstrom et al.*, 1999, 2000]. However, regional case studies have failed to detect a correlation between (^{230}Th)/(^{238}U) and Pb or Sr isotopes [*Bourdon et al.*, 1996b; *Sims et al.*, 2000]. A significant correlation between (^{230}Th)/(^{238}U) and radiogenic isotopes is observed in Hawaii, but *Stracke et al.* [1999] argued that this correlation is inconsistent with an important influence from pyroxenite in the Hawaiian source.

[49] Calculated (^{230}Th)/(^{238}U) as a function of upwelling rate for a fixed productivity of 16.5%/GPa and pyroxenite mineralogy similar to G2 pyroxenite are shown in Figure 10. The ^{230}Th excess is 1.22 at 5 cm/yr for partition coefficients appropriate for aluminous vacancy-rich cpx [*Pertermann and Hirschmann*, 2002]. Lithologies with less aluminous pyroxenes may have higher proportions of garnet than G2 pyroxenite. In these cases, the effect of more garnet could be partially mitigated by larger values U and Th partition coefficients in vacancy-poor cpx. For example, if a composition with 35% garnet had cpx partition coefficients similar to that determined by *Hauri et al.* [1994], the resulting in (^{230}Th)/(^{238}U) would be similar to that expected for G2 pyroxenite.

[50] Importantly, garnet pyroxenite produces larger excesses for any given upwelling rate than partial melting of spinel peridotite; e.g., at 5 cm/yr and reasonable adiabatic productivities (6.6–13.2%/GPa), spinel peridotite melting alone produces (^{230}Th)/(^{238}U) of 1.03–1.06 for the cpx partition coefficients of *Wood et al.* [1999] (Figure 9) and less for the *D*'s of *Salters and Longhi* [1999]. This implies that the pyroxenite contribution to basalt petrogenesis could

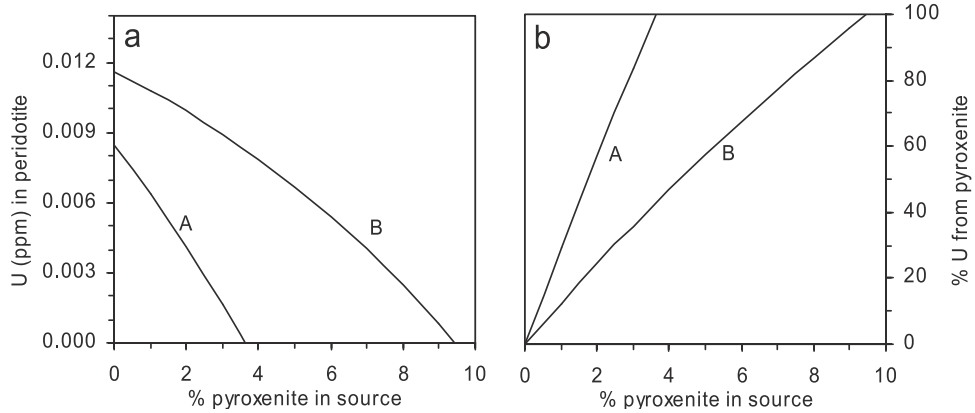

Figure 11. Calculation of the U budget of a mixed peridotite/pyroxenite mid-ocean ridge source, as explained in the text. (a) The concentration of U in peridotite is calculated assuming a source, which consists of a variable percentage of pyroxenite with a given U concentration and which generates 7 km of crust with a particular average concentration of U. In Curve "A," the pyroxenite has 0.136 ppm U and the average crust has 0.08 ppm U. In Curve "B," these values are 0.08 and 0.11, respectively. The amount of U that can be in the peridotite diminishes with increasing pyroxenite proportion in the source. (b) Calculation as in (a), but in this case the proportion of U in the crust, which derives from the pyroxenite, is shown. For modest proportions of pyroxenite in the source, a substantial fraction of the U comes from pyroxenite. Consequently, the aggregate melts will have $(^{230}Th)/(^{238}U)$ that is strongly influenced by the $(^{230}Th)/(^{238}U)$ of the pyroxenite-derived liquids.

indeed result in increased ^{230}Th excess if the pyroxenite is similar to G2.

[51] One reason that our calculations predict large ^{230}Th excesses from partial melts of garnet pyroxenite is that we employ small U and Th partition coefficients for aluminous, vacancy-rich cpx, as appropriate for the compositions observed in the G2 partial melting experiments [*Pertermann and Hirschmann*, 2002]. Larger partition coefficients dilute the effect of garnet, making the bulk D_{Th}/D_U closer to unity and thereby limiting development of ^{230}Th excesses. A second reason why significant ^{230}Th excesses are predicted is that we adopt small near-solidus productivities, based on melting relations of G2 (Figure 5). Because $(^{230}Th)/(^{238}U)$ is largely determined by conditions near the onset of partial melting [e.g., *McKenzie*, 1985], this difference is critical. We note that small near-solidus productivities are suitable for this quartz-bearing lithology, but may not be for other possible pyroxenite compositions. Therefore, provided that melt extraction from pyroxenite bodies can occur at low porosity and that the pyroxenite present has near-solidus melting relations similar to the G2 composition investigated here, we conclude that pyroxenite domains in basalt source regions can be the sources of elevated $(^{230}Th)/(^{238}U)$.

[52] Our conclusion regarding development of significant $(^{230}Th)/(^{238}U)$ from partial melting of garnet pyroxenite contrasts with that of *Stracke et al.* [1999]. *Stracke et al.* [1999] used the cpx partition coefficients for U and Th from the study of *Hauri et al.* [1994], which are nearly an order of magnitude larger than the ones we employ and which produce smaller $(^{230}Th/^{238}U)$ for otherwise equivalent conditions. Additionally, *Stracke et al.* [1999] assumed that initial melting of pyroxenite is rapid, which limits ingrowth of ^{230}Th.

[53] A key point is that the larger excesses developed from the pyroxenite should have a significant effect on aggregated melts, even if the total proportion of pyroxenite in the source is small, because the concentration of U is likely to be much larger in pyroxenite than in the peridotite and because pyroxenite partial melts are extracted from a larger volume of mantle than partial melts of peridotite [*Hirschmann and Stolper*, 1996]. After <1% partial melting, the inventory of U and Th in partial melts depend principally on their abundance in the source materials, and are unaffected by the relative extents of melting of those materials.

[54] Because concentrations of U in MORB are small, models which call on larger contributions of pyroxenite must have limited contributions of U from peridotite, such that aggregated melts have U similar to primitive MORB. *Jochum et al.* [1983] considered the U concentration of average depleted MORB to be 0.08 ppm, similar to the average U concentration, 0.11 ppm (n = 241), of MORB glasses with $\geq$8 wt.% MgO (PETDB) (http://petdb.ldeo.columbia.edu/petdb/). Taking these compositions and calculating mass balances for a regime that generates 7 km of crust (using the melting models from Figures 5 and 8) places limits on the concentration of U in the peridotite portion of a source. U concentrations in pyroxenite are poorly known, but *Hirschmann and Stolper* [1996] proposed concentrations for AVG and SOC pyroxenite of 0.085 and 0.136 ppm U, respectively. Depending on specific assumptions about pyroxenite and average crust compositions, the allowed concentration of U in the peridotite diminishes to zero for 4–10% pyroxenite in the source (Figure 11a); any greater abundances of pyroxenite would require that the pyroxenite either have less U or melt less productively.

[55] Using the mass balances developed in the previous paragraph, it is possible to calculate the proportion of U in the aggregated crust that originates in pyroxenite. A source with 2% pyroxenite contributes 24–57% of the U supplied

to the crust (Figure 11b). For sources assumed to be in secular equilibrium prior to melting, the same mass balances apply to ^{230}Th. Therefore for the Th/U fractionations depicted in Figure 10 and an upwelling rate of 5 cm/yr, spinel peridotite would give $(^{230}Th)/(^{238}U)$ of 1.04, but the same source with 2% of a G2-like pyroxenite would generate aggregated melts of 1.08–1.14. Thus small proportions of pyroxenite could have substantial impact on the U-series characteristics of aggregated MORB.

[56] We note that the relatively strong effect of pyroxenite on $(^{230}Th)/(^{238}U)$ may not necessarily be reflected in other isotope systems such as $^{87}Sr/^{86}Sr$ or $^{206}Pb/^{204}Pb$, as the enrichments of Sr and Pb are relatively modest (see section 4.2 above). This suggests that the absence of correlations between $(^{230}Th)/(^{238}U)$ and long-lived radiogenic isotopes in some MORB suites, as observed by *Bourdon et al.* [1996a, 1996b] and *Sims et al.* [2000], may not provide strong evidence for or against an important role for pyroxenite in U-series of MORB. *Lundstrom et al.* [2000] reached a similar conclusion from examination of trends between $^{87}Sr/^{86}Sr$ and Th/U in MORB.

6. Concluding Remarks

[57] Our experimental data show that basaltic fertile pyroxenite melts at significantly lower temperature than normal peridotite at a given pressure. Thus, if present in upwelling mantle, pyroxenite heterogeneities melt at greater depth than the surrounding peridotite. Due to its high average melting rate the pyroxenite is likely to melt to a large degree before the peridotite solidus is reached. This, in combination with the low observed garnet modes in the pyroxenite, limits the in situ trace element fractionations of pyroxenite, and so the ''garnet signature'' imparted to MORB from partial melting of this type of pyroxenite is modest. Although the pyroxenite has a high average melt productivity, and smaller garnet mode than previously expected for basaltic bulk compositions, the near-solidus melting rate can be low enough to produce strongly elevated $(^{230}Th)/(^{238}U)$. Mixing of peridotite-derived and garnet pyroxenite-derived melts in basalt source regions could therefore result in overall elevated $(^{230}Th)/(^{238}U)$, for both MORB and OIB.

[58] **Acknowledgments.** We thank H.-G. Stosch for the sample of eclogite W6.8 and M. B. Baker for a copy of his mass balance program. D. Xirouchakis and J. Simpson are thanked for their efforts maintaining the piston-cylinder lab. Discussions with T. Kogiso, and helpful reviews by J. Longhi, C. Lundstrom, and M. Walter are much appreciated. This research is supported by NSF grants OCE9706526 and OCE9876255 and a University of Minnesota grant-in-aid to M.M.H.

References

Albarede, F., and A. Provost, Petrological and geochemical mass-balance equations: An algorithm for least-square fitting and general error analysis, *Comput. Geosci.*, *3*, 309–326, 1977.

Allègre, C. J., and D. L. Turcotte, Implications of a two component marble cake mantle, *Nature*, *323*, 123–127, 1986.

Asimow, P. D., M. M. Hirschmann, and E. M. Stolper, An analysis of variations in isentropic melt productivity, *Philos. Trans. R. Soc. London, Ser. A*, *355*, 255–281, 1997.

Asimow, P. D., M. M. Hirschmann, and E. M. Stolper, Calculation of peridotite partial melting from thermodynamic models of minerals and melts, 4, Adiabatic decompression and the composition and mean properties of mid-ocean ridge basalts, *J. Petrol.*, *42*, 963–998, 2001.

Baker, M. B., and E. M. Stolper, Determining the composition of high-pressure mantle melts using diamond aggregates, *Geochim. Cosmochim. Acta*, *58*, 2811–2827, 1994.

Beattie, P., Uranium-thorium disequilibria and partitioning on melting of garnet peridotite, *Nature*, *363*, 63–65, 1993.

Bender, J. F., C. H. Langmuir, and G. H. Hanson, Petrogenesis of basalt glasses from the Tamayo region, East Pacific Rise, *J. Petrol.*, *25*, 213–254, 1984.

Bodinier, J. L., M. Guiraud, J. Fabriés, J. Dostal, and C. Dupuy, Petrogenesis of layered pyroxenites from the Lherz, Freychinède and Prades ultramafic bodies (Ariège, French Pyrénées), *Geochim. Cosmochim. Acta*, *51*, 279–290, 1987.

Blundy, J. D., J. A. C. Robinson, and B. J. Wood, Heavy REE are compatible in clinopyroxene on the spinel lherzolite solidus, *Earth Planet. Sci. Lett.*, *160*, 493–504, 1998.

Bourdon, B., A. Zindler, T. Elliott, and C. H. Langmuir, Constraints on mantle melting at mid-ocean ridges from global ^{238}U-^{230}Th disequilibrium data, *Nature*, *384*, 231–235, 1996a.

Bourdon, B., C. H. Langmuir, and A. Zindler, Ridge-hotspot interaction along the Mid-Atlantic Ridge between 37°30′ and 40°30′ N: The U-Th disequilibrium, *Earth Planet. Sci. Lett.*, *142*, 175–189, 1996b.

Carlson, R. W., and G. M. Nowell, Olivine-poor sources for mantle derived magmas: Os and Hf isotope evidence from potassic magmas of the Colorado Plateau, *Geochem. Geophys. Geosyst.*, *2*, 10.1029/2000GC000128, 2001.

Carswell, D. A., (ed.), *Eclogite Facies Rocks*, Chapman and Hall, New York, 1990.

Chabaux, F., and C. J. Allegre, ^{238}U-^{230}Th-^{226}Ra disequilibria in volcanics: A new insight into melting conditions, *Earth Planet. Sci. Lett.*, *126*, 61–74, 1994.

Chadam, J., D. Hoff, P. Ortoleva, and A. Sen, Reactive-infiltration instability, *J. Appl. Math.*, *36*, 207–238, 1976.

Clarke, G. L., J. C. Aitchison, and D. Cluzel, Eclogites and blueschists of the Pam Peninsula, NE New Caledonia: A reappraisal, *J. Petrol.*, *38*, 843–876, 1997.

Condomines, M., and O. Sigmarsson, ^{238}U-^{230}Th disequilibria and mantle melting processes: A discussion, *Chem. Geol.*, *162*, 95–104, 2000.

Cordery, M. J., G. F. Davies, and I. H. Campbell, Genesis of flood basalts from eclogite-bearing mantle plumes, *J. Geophys. Res.*, *102*, 20,179–20,197, 1997.

Daines, M. J., and D. L. Kohlstedt, A laboratory study of melt migration, *Philos. Trans. R. Soc. London, Ser. A*, *342*, 43–52, 1993.

Dardon, A., M. W. Schmidt, G. Chazot, M. Tiepolo, and R. Vannucci, Rutile/mineral and rutile/liquid partition coefficients for HFSE, REE and actinides: Results from natural eclogites and partial melting experiments, in *Eleventh Annual Goldschmidt Conference*, abstract 3630, LBI, contrib. 1088, CD-ROM, Lunar and Planet. Inst., Houston, 2001.

DiVinzenzo, G., R. Palmeri, F. Talarico, P. A. M. Andriessen, and C. A. Ricci, Petrology and geochronology of eclogites from the Lanterman Range, Antarctica, *J. Petrol.*, *38*, 1391–1417, 1997.

Dick, H. J. B., S. H. Bloomer, S. H. Kirby, D. S. Stakes, and C. K. Mawer, Lithostratigraphic evolution of an in-situ section of oceanic layer 3, in *Proc. Ocean Drill. Program Sci. Results*, vol. 118, edited by R. P. Von Herzen et al., pp. 439–538, Ocean Drill. Program, College Station, Tex., 1991.

Eiler, J. M., P. Schiano, N. Kitchen, and E. M. Stolper, Oxygen-isotope evidence for recycled crust in the sources of mid-ocean-ridge basalts, *Nature*, *403*, 530–534, 2000.

Falloon, T. J., and L. V. Danyushevsky, Melting of refractory mantle at 1.5, 2 and 2.5 GPa under anhydrous and H_2O-undersaturated conditions: Implications for the petrogenesis of high-Ca boninites and the influence of subduction components on mantle melting, *J. Petrol.*, *41*, 257–283, 2000.

Feigenson, M. D., and M. J. Carr, The source of Central American lavas: Inferences from geochemical inverse modeling, *Contrib. Mineral. Petrol.*, *113*, 226–235, 1993.

Frey, F. A., N. Walker, D. Stakes, S. R. Hart, and R. Nielsen, Geochemical characteristics of basalt glasses from the AMAR and FAMOUS axial valleys, Mid-Atlantic Ridge (36°–37°N): Petrogenetic implications, *Earth Planet. Sci. Lett.*, *115*, 117–136, 1993.

Gaetani, G. A., and E. B. Watson, Trace element partitioning near the peridotite solidus: The importance of melt structure, *Eos Trans. AGU*, *81*, F13832000.

Gillis, K. M., et al., Site 895, in *Proc. Ocean Drill. Program Initial Report*, vol. 147, edited by K. M. Gillis et al., pp. 109–157, Ocean Drill. Program, College Station, Tex., 1993.

Hamelin, B., and C. J. Allègre, Lead isotope study of orogenic lherzolite massifs, *Earth Planet. Sci. Lett.*, *91*, 117–131, 1988.

Harlow, G. E., Interpretation of Kcpx and CaEs components in clinopyroxene from diamond inclusions and mantle samples, *Proc. Int. Kimberlite Conf.*, *7*, 321–331, 1999.

Hauri, E. H., Major-element variability in the Hawaiian mantle plume, *Nature*, *382*, 415–419, 1996.

Hauri, E. H., Melt migration and mantle chromatography, 1, Simplified theory and conditions for chemical and isotopic decoupling, *Earth Planet. Sci. Lett.*, *153*, 1–19, 1997.

Hauri, E. H., T. P. Wagner, and T. L. Grove, Experimental and natural partitioning of Th, U, Pb and other trace elements between garnet, clinopyroxene and basaltic melts, *Chem. Geol.*, *117*, 149–166, 1994.

Hekinian, R., D. Bideau, J. Francheteau, J. L. Cheminee, R. Armijo, P. Lonsdale, and N. Blum, Petrology of the East Pacific Rise crust and upper mantle exposed in Hess Deep (eastern Equatorial Pacific), *J. Geophys. Res.*, *98*, 8069–8094, 1993.

Herzberg, C., P. Raterron, and J. Zhang, New experimental observations on the anhydrous solidus for peridotite KLB-1, *Geochem. Geophys. Geosyst.*, *1*, 10.1029/2000GC000089, 2000.

Hirose, K., and I. Kushiro, Partial melting of dry peridotites at high pressure: Determination of compositions of melts segregated from peridotites using aggregates of diamonds, *Earth Planet. Sci. Lett.*, *114*, 477–489, 1993.

Hirschmann, M. M., Mantle solidus: Experimental constraints and the effects of peridotite composition, *Geochem. Geophys. Geosyst.*, *1*, 10.1029/2000GC000070, 2000.

Hirschmann, M. M., and E. M. Stolper, A possible role for garnet pyroxenite in the origin of the "garnet signature" in MORB, *Contrib. Mineral. Petrol.*, *124*, 185–208, 1996.

Hirschmann, M. M., M. B. Baker, and E. M. Stolper, Partial melting of mantle pyroxenite, *Eos Trans. AGU*, *76*, F696, 1995.

Hirschmann, M. M., M. S. Ghiorso, and E. M. Stolper, Calculation of peridotite partial melting from thermodynamic models of minerals and melts, 3, Controls on isobaric melt productivity and the effect of water on melt, *J. Petrol.*, *40*, 831–851, 1999.

Hirth, G., and D. L. Kohlstedt, Water in the oceanic upper mantle: Implications for rheology, melt extraction and the evolution of the lithosphere, *Earth Planet. Sci. Lett.*, *144*, 93–108, 1996.

Hofmann, A. W., Chemical differentiation of the Earth: The relationship between mantle, continental crust, and oceanic crust, *Earth Planet. Sci. Lett.*, *90*, 297–314, 1988.

Hofmann, A. W., and S. R. Hart, An assessment of local and regional isotopic equilibrium in the mantle, *Earth Planet. Sci. Lett.*, *38*, 44–62, 1978.

Hofmann, A. W., and W. M. White, Mantle plumes from ancient oceanic crust, *Earth Planet. Sci. Lett.*, *57*, 421–436, 1982.

Ita, J., and L. Stixrude, Petrology, elasticity, and composition of the mantle transition zone, *J. Geophys. Res.*, *97*, 6849–6866, 1992.

Jochum, K. P., A. W. Hofmann, E. Ito, H. M. Seufert, and W. M. White, K, U, and Th in mid-ocean ridge basalt glasses and heat production, K/U and K/Rb in the mantle, *Nature*, *306*, 431–436, 1983.

Johnston, A. D., Anhydrous P-T phase relations of near-primary high-alumina basalt from the South Sandwich Islands, *Contrib. Mineral. Petrol.*, *92*, 368–382, 1986.

Kamber, B. S., and K. D. Collerson, Role of "hidden" deeply subducted slabs in mantle depletion, *Chem. Geol.*, *166*, 241–254, 2000.

Kelemen, P. B., J. A. Whitehead, E. Aharonov, and K. A. Jordahl, Experiments on flow focusing in soluble porous media, with applications to melt extraction from the mantle, *J. Geophys. Res.*, *100*, 475–496, 1995.

Kennedy, A. K., G. E. Lofgren, and G. J. Wasserburg, An experimental study of trace-element partitioning between olivine, orthopyroxene and melt in chondrules-equilibrium value and kinetic effects, *Earth Planet. Sci. Lett.*, *115*, 177–195, 1993.

Kinzler, R. J., Melting of mantle peridotite at pressures approaching the spinel to garnet transition: Application to mid-ocean ridge basalt petrogenesis, *J. Geophys. Res.*, *102*, 853–874, 1997.

Kinzler, R. J., and T. L. Grove, Primary magmas of mid-ocean ridge basalts, 2, Applications, *J. Geophys. Res.*, *97*, 6097–6926, 1992.

Kogiso, T., Y. Tatsumi, and S. Nakano, Trace element transport during dehydration processes in the subducted oceanic crust, 1, Experiments and implications for the origin of ocean island basalts, *Earth Planet. Sci. Lett.*, *148*, 193–205, 1997a.

Kogiso, T., Y. Tatsumi, G. Shimoda, and H. G. Barsczus, High μ [HIMU] ocean island basalts in southern Polynesia: New evidence for whole mantle scale recycling of subducted oceanic crust, *J. Geophys. Res.*, *102*, 8085–8103, 1997b.

Kogiso, T., M. M. Hirschmann, and P. W. Reiners, Constraints from isotopic variations on the physical dimensions of chemical heterogeneities in oceanic basalt source regions, *Eos Trans. AGU*, *81*, F1280, Fall Meet. Suppl., 2000.

Kogiso, T., M. M. Hirschmann, and D. J. Frost, Partial melting experiments of Mg-rich garnet clinopyroxenite and the origin of HIMU basalts, *Eos Trans. AGU*, *81*, S429–S430, Fall Meet. Suppl., 2001.

Langmuir, C. H., E. M. Klein, and T. Plank, Petrological systematics of mid-ocean ridge basalts: Constraints on melt generation beneath ocean ridges, *Geophys. Monogr. AGU*, *71*, 183–280, 1992.

Leeman, W. P., and D. L. Harry, A binary source model for extension-related magmatism in the Great Basin, western North America, *Science*, *262*, 1550–1554, 1993.

Lundstrom, C. C., J. Gill, Q. Williams, and M. Perfit, Mantle melting and basalt extraction by equilibrium porous flow, *Science*, *270*, 1958–1961, 1995.

Lundstrom, C. C., D. E. Sampson, M. R. Perfit, J. Gill, and Q. Williams, Insights into mid-ocean ridge basalt petrogenesis: U-series disequilibria from the Siqueiros Transform, Lamont Seamounts, and the East Pacific Rise, *J. Geophys. Res.*, *104*, 13,013–13,024, 1999.

Lundstrom, C. C., J. Gill, and Q. Williams, A geochemically consistent hypothesis for MORB generation, *Chem. Geol.*, *162*, 105–126, 2000.

McCormick, T. C., Crystal-chemical aspects of non-stoichiometric pyroxenes, *Am. Mineral.*, *71*, 1434–1440, 1986.

McCulloch, M. T., and J. A. Gamble, Geochemical and geodynamical constraints on subduction zone magmatism, *Earth Planet. Sci. Lett.*, *102*, 358–374, 1991.

McKenzie, D., (^{230}Th-^{238}U) disequilibrium and the melting process beneath ridge axes, *Earth Planet. Sci. Lett.*, *72*, 149–157, 1985.

Niu, Y. L., and R. Batiza, Trace element evidence from seamounts for recycled oceanic crust in the Eastern Pacific mantle, *Earth Planet. Sci. Lett.*, *148*, 471–483, 1997.

Pearson, D. G., G. R. Davies, and P. H. Nixon, Geochemical constraints on the petrogenesis of diamond facies pyroxenites from the Beni Bousera peridotite massif, *J. Petrol.*, *34*, 125–172, 1993.

Pertermann, M., and M. M. Hirschmann, Trace element partitioning between vacancy-rich eclogitic clinopyroxene and silicate melt, *Am. Mineral.*, *87*, 1365–1376, 2002.

Phipps Morgan, J., Isotope topography of individual hotspot basalt arrays: Mixing curves or melt extraction trajectories?, *Geochem. Geophys. Geosyst.*, *1*, 10.1029/1999GC000004, 1999.

Phipps Morgan, J., Thermodynamics of pressure release melting of a veined plum pudding mantle, *Geochem. Geophys. Geosyst.*, *2*, 10.1029/2000GC000049, 2001.

Phipps Morgan, J., and W. J. Morgan, Two-stage melting and the geochemical evolution of the mantle: A recipe for mantle plum-pudding, *Earth Planet. Sci. Lett.*, *170*, 215–239, 1999.

Pickering-Witter, J. M., and A. D. Johnston, The effects of variable mineral proportions on the melting systematics of fertile peridotitic assemblages, *Contrib. Mineral. Petrol.*, *140*, 190–211, 2000.

Plank, T., and C. H. Langmuir, Effects of the melting regime on the composition of the oceanic crust, *J. Geophys. Res.*, *97*, 19,749–19,770, 1992.

Rapp, R. P., and E. B. Watson, Dehydration melting of metabasalt at 8–32 kbar: Implications for continental growth and crust-mantle recycling, *J. Petrol.*, *36*, 891–931, 1995.

Robinson, J. A. C., and B. J. Wood, The depth of the spinel to garnet transition at the peridotite solidus, *Earth Planet. Sci. Lett.*, *164*, 277–284, 1999.

Robinson, J. A. C., B. J. Wood, and J. D. Blundy, The beginning of melting of fertile and depleted peridotite at 1.5 GPa, *Earth Planet. Sci. Lett.*, *155*, 97–111, 1998.

Sack, R. O., and M. S. Ghiorso, Thermodynamics of multicomponent pyroxenes, 1, Formulation of a general model, *Contrib. Mineral. Petrol.*, *116*, 277–286, 1994.

Salters, V. J. M., and S. R. Hart, The Hf-paradox and the role of garnet in the MORB source, *Nature*, *342*, 420–422, 1989.

Salters, V. J. M., and J. Longhi, Trace element partitioning during the initial stages of melting beneath mid-ocean ridges, *Earth Planet. Sci. Lett.*, *166*, 15–30, 1999.

Schiano, P., J. M. Eiler, I. D. Hutcheon, and E. M. Stolper, Primitive CaO-rich, silica undersaturated melts in island arcs: Evidence for the involvement of clinopyroxene-rich lithologies in the petrogenesis of arc magmas, *Geochem. Geophys. Geosyst.*, *1*, 10.1029/1999GC000032, 2000.

Shen, Y., and D. W. Forsyth, Geochemical constraints on initial and final depths of melting beneath mid-ocean ridges, *J. Geophys. Res.*, *100*, 2211–2237, 1995.

Sims, K. W., J. Blichert-Toft, and M. Perfit, Melting beneath the East Pacific Rise, 9°–10°N: Implications from combined Nd-Hf-Sr-Th isotopic measurements, *J. Conf. Abstr.*, *5*(2), 930, 2000.

Sims, K. W. W., D. J. DePaolo, M. T. Murrell, W. S. Baldridge, S. Goldstein, D. Clague, and M. Jull, Porosity of the melting zone and variations in the solid mantle upwelling rate beneath Hawaii: Inferences from ^{238}U-^{230}Th-^{226}Ra and ^{235}U-^{231}Pa disequilibria, *Geochim. Cosmochim. Acta*, *63*, 4119–4138, 1999.

Sisson, V. B., I. E. Ertan, and H. G. Ave' Lallement, High pressure ($\sim$2000 MPa) kyanite- and glaucophane-bearing pelitic schist and eclogite from Cordillera de la Costa Belt, Venezuela, *J. Petrol.*, *38*, 65–83, 1997.

Sleep, N. H., Tapping of magmas from ubiquitous mantle heterogeneities: An alternative to mantle plumes?, *J. Geophys. Res.*, *89*, 10,029–10,041, 1984.

Smyth, J. R., Cation vacancies and the crystal chemistry of breakdown reactions in kimberlitic omphacites, *Am. Mineral.*, *65*, 1185–1191, 1980.

Snyder, G. A., L. A. Taylor, G. Crozaz, A. N. Halliday, B. L. Beard, V. N. Sobolev, and N. V. Sobolev, The origins of Yakutian eclogite xenoliths, *J. Petrol.*, *38*, 85–113, 1997.

Spiegelman, M., and T. Elliott, Consequences of melt transport for uranium series disequilibrium in young lavas, *Earth Planet. Sci. Lett.*, *118*, 1–20, 1993.

Stosch, H. G., and G. W. Lugmair, Geochemistry and evolution of MORB-type eclogites from the Münchberg Massif, southern Germany, *Earth Planet. Sci. Lett.*, *99*, 230–249, 1990.

Stracke, A., V. J. M. Salters, and K. W. W. Sims, Assessing the presence of garnet-pyroxenite in the mantle sources of basalts through combined hafnium-neodymium-thorium isotope systematics, *Geochem. Geophys. Geosyst.*, *1*, 10.1029/1999GC000013, 1999.

Suen, C. J., and F. A. Frey, Origins of the mafic and ultramafic rocks in the Ronda peridotite, *Earth Planet. Sci. Lett.*, *85*, 183–202, 1988.

Takahashi, E., K. Nakajima, and T. L. Wright, Origin of the Columbia River basalts: Melting model of a heterogeneous plume head, *Earth Planet. Sci. Lett.*, *162*, 63–80, 1998.

Toomey, D. R., W. S. D. Wilcock, S. C. Solomon, W. C. Hammond, and J. A. Orcutt, Mantle seismic structure beneath the MELT region of the East Pacific Rise from P and S wave tomography, *Science*, *280*, 1224–1227, 1998.

Van Westrenen, W., J. Blundy, and B. Wood, Crystal-chemical controls on trace element partitioning between garnet and anhydrous silicate melt, *Am. Mineral.*, *84*, 838–847, 1999.

Van Westrenen, W., J. D. Blundy, and B. J. Wood, High field strength element/rare earth element fractionation during partial melting in the presence of garnet: Implications for identification of mantle heterogeneities, *Geochem. Geophys. Geosyst.*, *2*, 10.1029/2000GC000133, 2001.

Walter, M. J., Melting of garnet peridotite and the origin of komatiite and depleted lithosphere, *J. Petrol.*, *39*, 29–60, 1998.

Weaver, B. L., The origin of ocean island basalt end-member compositions: Trace element and isotopic constraints, *Earth Planet. Sci. Lett.*, *104*, 381–397, 1991.

White, R. S., D. McKenzie, and R. K. O'Nions, Oceanic crustal thickness from seismic measurements and rare earth element inversions, *J. Geophys. Res.*, *97*, 19,683–19,715, 1992.

Williams, R. M., and J. B. Gill, Effects of partial melting on the uranium decay series, *Geochim. Cosmochim. Acta*, *53*, 1607–1619, 1989.

Wood, B. J., and C. M. B. Henderson, Compositions and unit-cell parameters of synthetic non-stoichiometric tschermakitic clinopyroxenes, *Am. Mineral.*, *63*, 66–72, 1978.

Wood, B. J., J. D. Blundy, and J. A. C. Robinson, The role of clinopyroxene in generating U-series disequilibrium during mantle melting, *Geochim. Cosmochim. Acta*, *63*, 1613–1620, 1999.

Xirouchakis, D., M. M. Hirschmann, and J. A. Simpson, The effect of titanium on the silica content and on mineral-liquid partitioning of mantle-equilibrated melts, *Geochim. Cosmochim. Acta*, *65*, 2201–2217, 2001.

Yasuda, A., and T. Fujii, Ascending subducted oceanic crust entrained within mantle plumes, *Geophys. Res. Lett.*, *25*, 1561–1564, 1998.

Yasuda, A., T. Fujii, and K. Kurita, Melting phase relations of an anhydrous mid-ocean ridge basalt from 3 to 20 GPa: Implications for the behavior of subducted oceanic crust in the mantle, *J. Geophys. Res.*, *99*, 9401–9414, 1994.

Yaxley, G. M., Experimental study of the phase and melting relations of homogeneous basalt + peridotite mixtures and implications for the petrogenesis of flood basalts, *Contrib. Mineral. Petrol.*, *139*, 326–338, 2000.

Yaxley, G. M., and D. H. Green, Reactions between eclogite and peridotite: Mantle refertilization by subduction of oceanic crust, *Schweiz. Mineral. Petrogr. Mitt.*, *78*, 243–255, 1998.

Zindler, A., and S. R. Hart, Chemical geodynamics, *Annu. Rev. Earth Planet. Sci. Lett.*, *14*, 493–571, 1986.

Zindler, A., H. Staudigel, and R. Batiza, Isotope and trace element geochemistry of young Pacific seamounts: Implications for the scale of upper mantle heterogeneity, *Earth Planet. Sci. Lett.*, *70*, 175–195, 1984.

M. M. Hirschmann, Department of Geology and Geophysics, University of Minnesota, 108 Pillsbury Hall, 310 Pillsbury Drive SE, Minneapolis, MN 55455, USA.

M. Pertermann, Institut für Mineralogie und Petrographie, Eidgenössische Technische Hochschule, CH-8092 Zürich, Switzerland. (maik.pertermann@erdw.ethz.ch)